

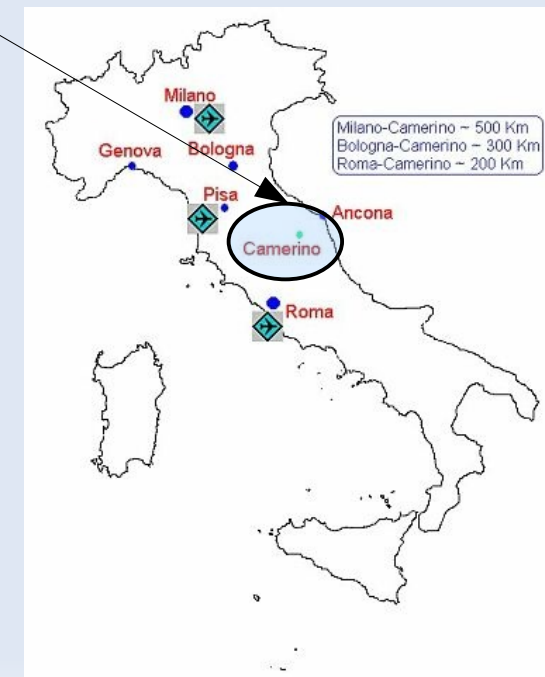
X-ray absorption and fluorescence spectroscopy: the EXAFS technique



SOCIETÀ ITALIANA LUCE DI SINGROTRONE
ITALIAN SYNCHROTRON RADIATION SOCIETY
www.synchrotron-radiation.it

Andrea Di Cicco

*Physics Division, School of Science and Technology,
Università di Camerino*



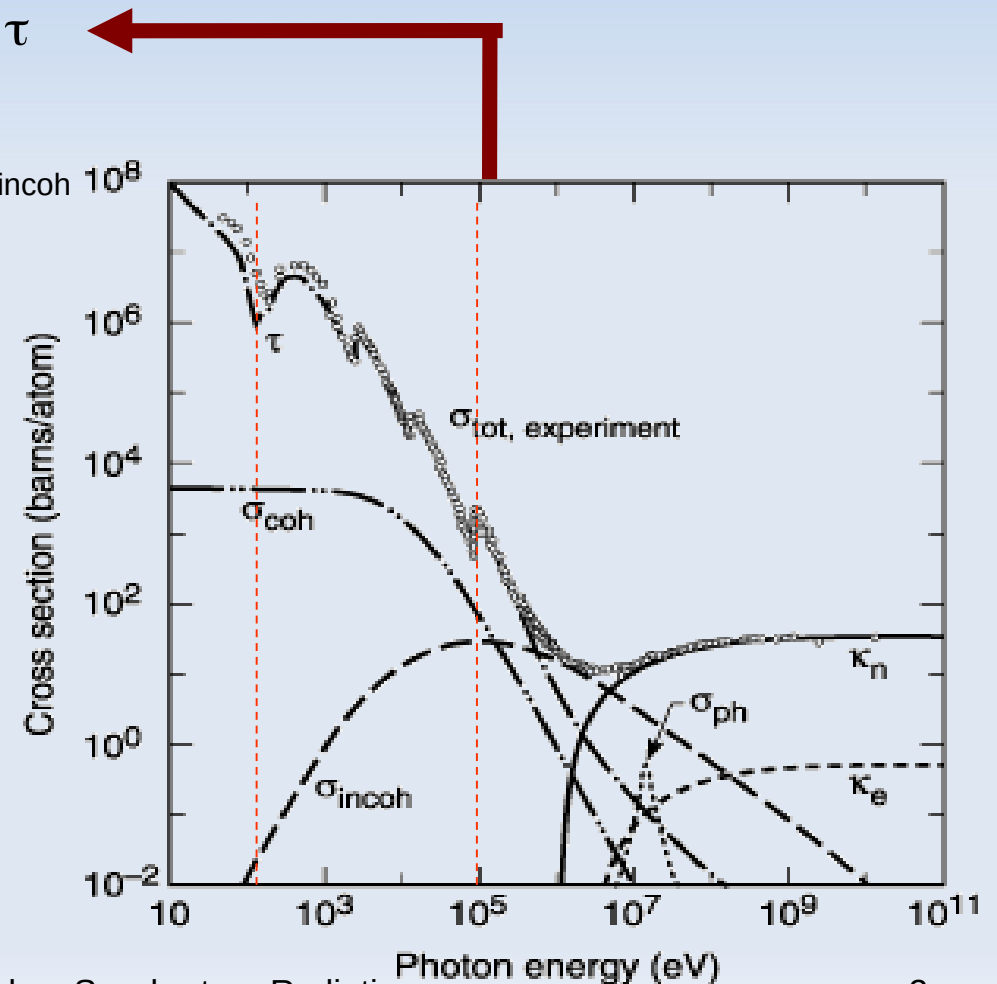
Photon-matter interaction processes

Light-matter interaction:

- photoelectric effect (absorption), τ
- elastic scattering (Rayleigh), σ_{coh}
- inelastic scattering (Compton), σ_{incoh}
- pair production, $e^- - e^+$, κ

Photoelectric absorption is the dominant effect in the x-ray range

$E = 0.1\text{keV}$ to 100keV
 $\lambda = 100 \text{ \AA}$ to 0.1 \AA



Photoelectric absorption

The absorption coefficient $\mu(\omega)$ can be expressed (in S.I. units) as

$$\mu(\omega) = n \sigma_a(\hbar\omega) = (2\hbar/\varepsilon_0\omega A_0^2 c) n \sum_f w_{fi},$$

Edge:	M _V	M _{IV}	M _{III}	M _{II}	M _I	L _{III}	L _{II}	L _I	K
Core level:	3d _{5/2}	3d _{3/2}	3p _{3/2}	3p _{1/2}	3s	2p _{3/2}	2p _{1/2}	2s	1s

where n is the number of atoms per unit volume, σ_a is the atomic absorption cross section, $\varepsilon_0\omega A_0^2 c/2\hbar$ is the photon flux (A_0 is the magnitude of the vector potential of the electromagnetic field) and w_{fi} is the probability of transition per unit time (transition rate) from the initial state $|\Psi_i\rangle$ to the final state $|\Psi_f\rangle$.

$$\Phi = \Phi_0 \exp[-\mu(\omega)x],$$

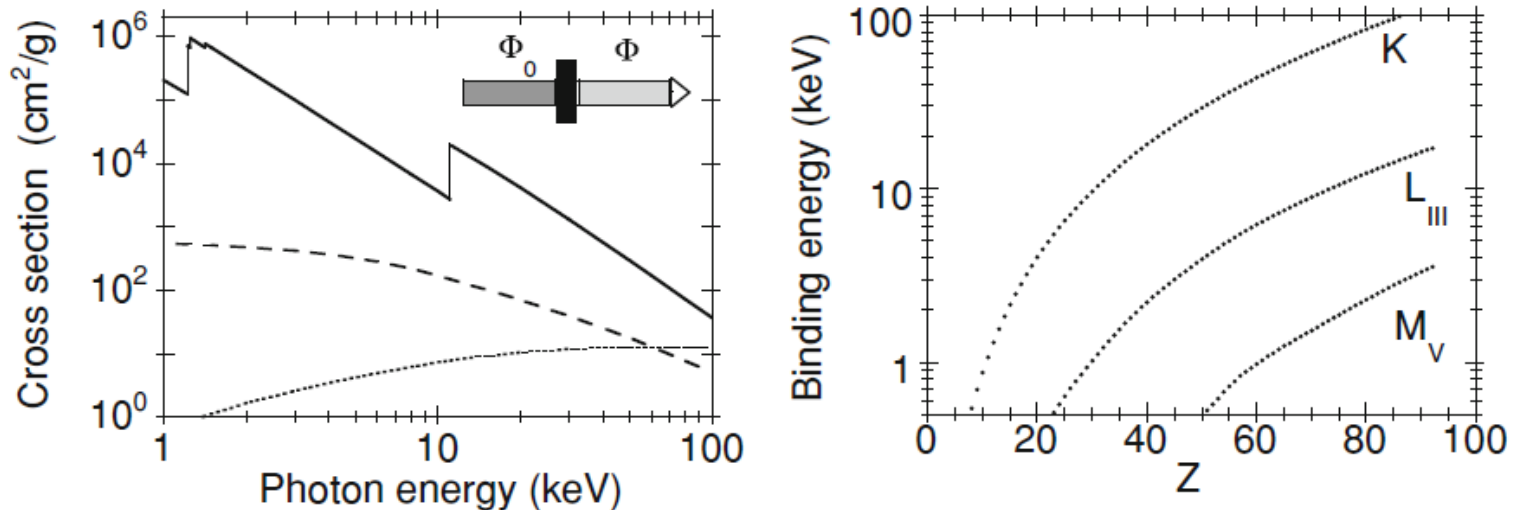
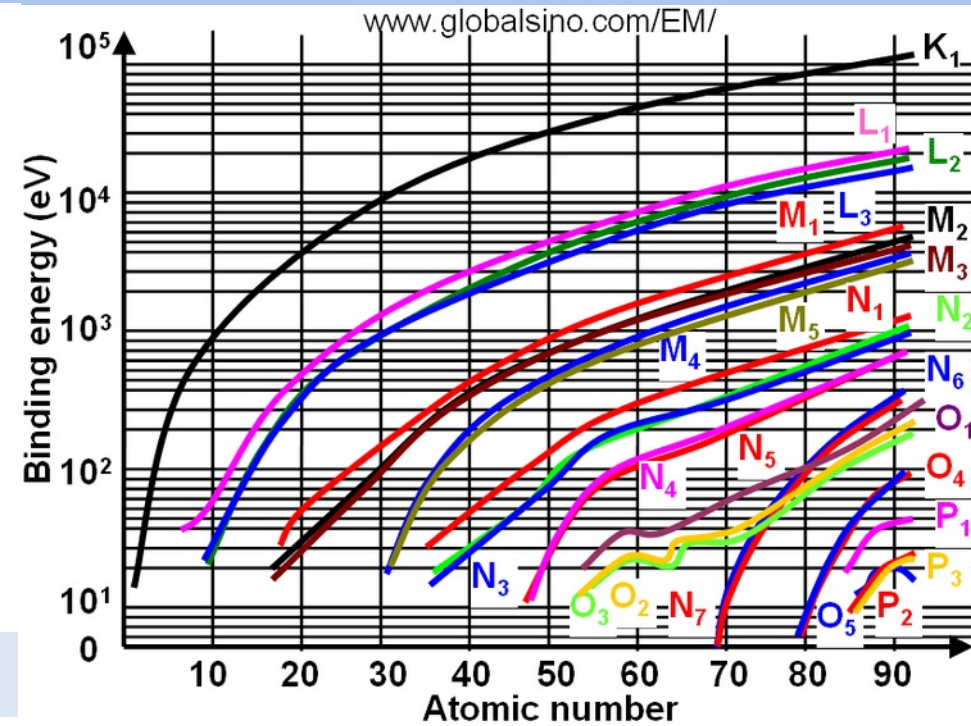
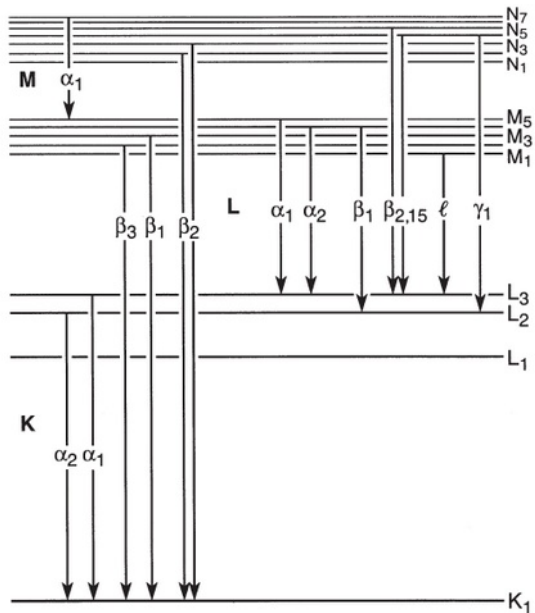


Fig. 6.1 *Left* X-ray absorption cross-sections for Germanium. *Continuous line* photoelectric absorption, with the three L edges (1.217, 1.248 and 1.414 keV) and the K edge (11.103 keV); *dashed line* elastic Thomson scattering; *dotted line* inelastic Compton scattering. *Right* Binding energy of the levels K, L_{III} e M_V as a function of the atomic number Z

The one-electron picture

- The phenomenon of X-ray absorption is mainly associated with core electron excitations.
- The K, L ... threshold sequence suggests it is mostly a one-electron phenomenon.
- Relevant matrix element $\langle \Psi_i | \epsilon \cdot \hat{p} | \Psi_f \rangle$
- Typical transition times 10^{-15} s (instantaneous with respect to atomic motion).



Characteristic energies

Each element has a characteristic set of excitation and fluorescence energies.

Iron: $Z=26$

Edge	Energy (eV)	Line	Transition	Energy (eV)	Strength
K	7112	K α_1	K-L3	6405.2	0.580
L3	706.8	K α_2	K-L2	6392.1	0.294
L2	719.9	K β_1	K-M3	7059.3	0.082
L1	844.6	K β_3	K-M2	7059.3	0.043
		K β_5	K-M4,5	7110.0	0.001

The fine structure

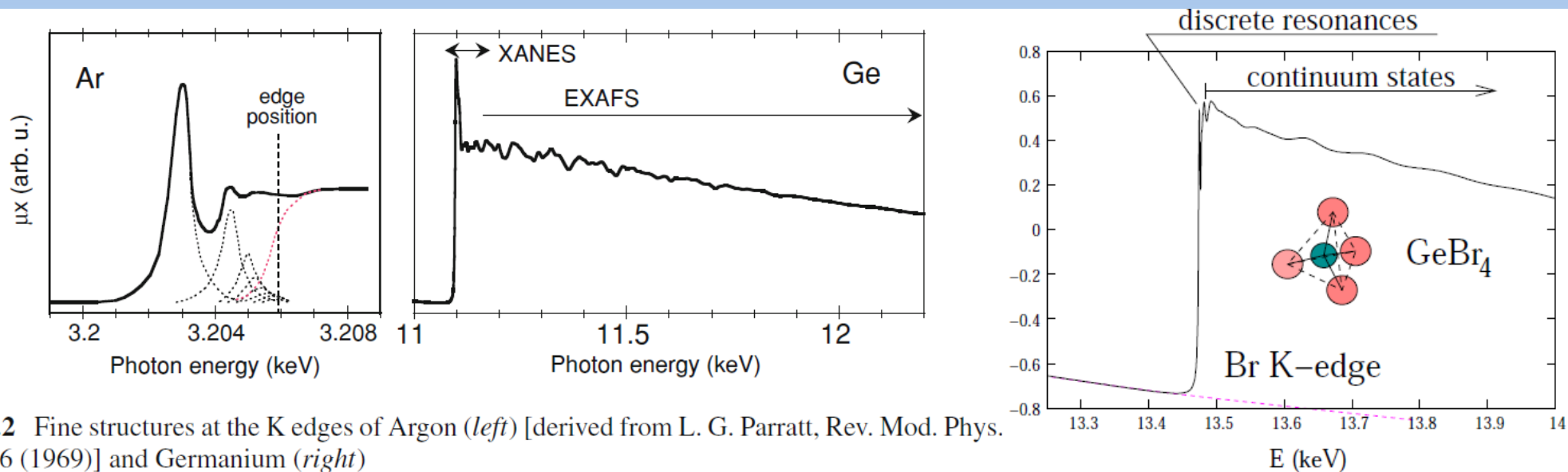


Fig. 6.2 Fine structures at the K edges of Argon (*left*) [derived from L. G. Parratt, Rev. Mod. Phys. 31, 616 (1969)] and Germanium (*right*)

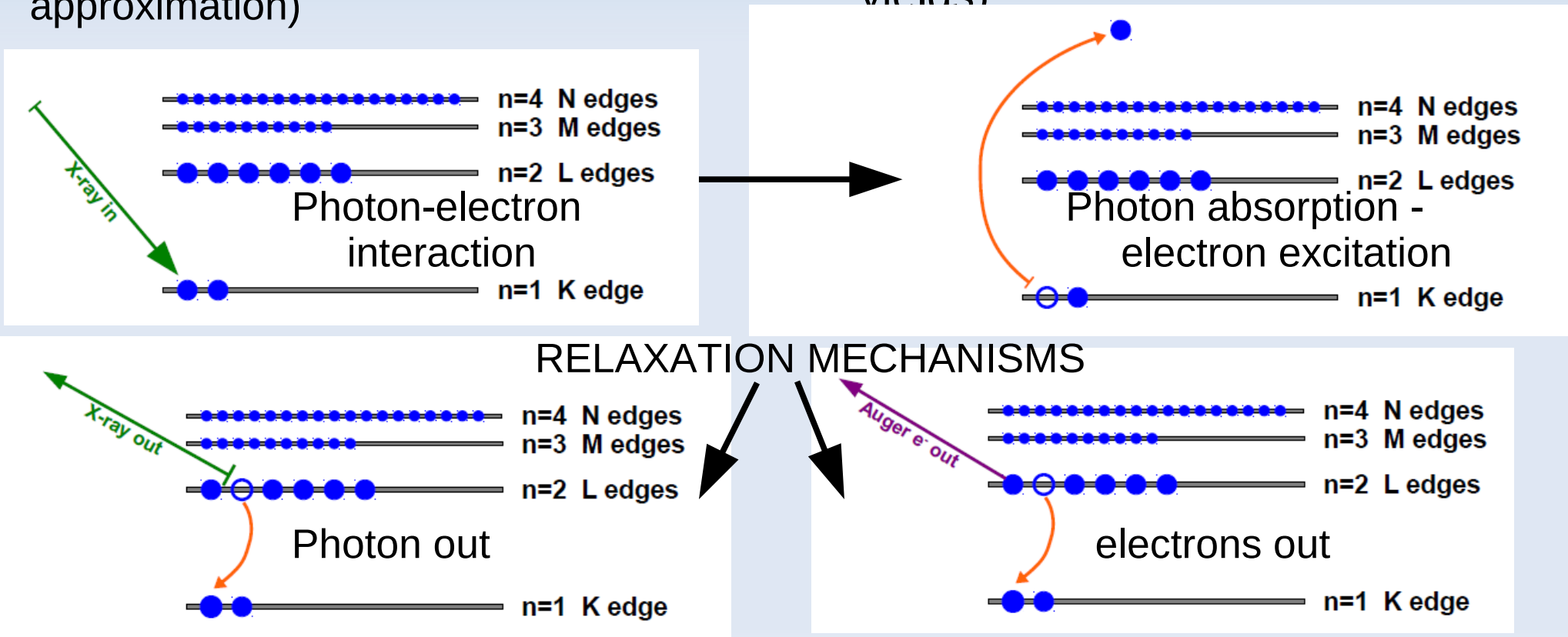
- A probe for average properties around the selected photoabsorber atomic species:
 - unoccupied density of **electronic states** (projected + excitonic effect)
 - short-range structure** (partial radial distribution functions)
- Can be indifferently applied to **gas, liquid and solid** (amorphous or crystalline) phases
- Suitable for investigations under **extreme thermodynamic conditions** (HP-HT)
- Full bulk sensitivity: typical sample thickness 0.01–10 mm

Fine structures first reported in 1920 by Kossel

XAS and XRF

- X-ray Absorption Spectroscopy (XAS) and X-Ray Fluorescence spectroscopy (XRF) are inner-shell spectroscopies (the x-ray photon interacts primarily with a deep-core electron – single electron approximation)

- *Spectroscopy* here means that we are measuring specific physical observables as a function of the photon energy (photon transmittance, fluorescence intensity, electron yields)



X-ray absorption in transmission mode

It is the preferred method for XAS experiments in the hard x-ray range for accurate, reliable and low-noise measurements

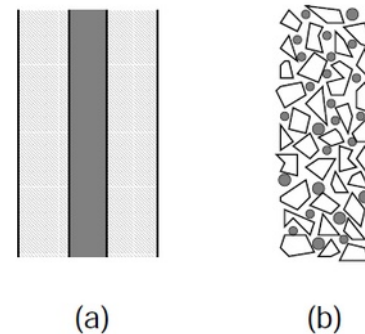
High flux of photons (synchrotron) → high counting rates, low noise (better than 10^4 signal to noise ratio)

Linear detectors in a wide range (ionization chambers)
Tricks of the trade (many)

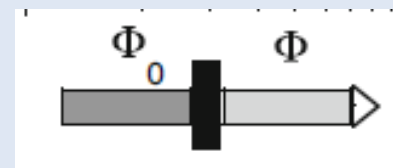
Sample of appropriate uniform thickness (micrometric-calculated for optimal absorption jumps)

Optimal setting of the beamline (pressure and gas of ionization chambers, collimation and positioning of the beam at sample position) +
.....many

The sample is usually dispersed (b) into a "chemically inert" matrix, low x-ray absorbing and high-temperature resistant (like BN, C, Al_2O_3 , ZrO_2). Micrometric powders of pure materials can be undercooled quite easily hundreds Celsius below the melting point.



$$\Phi = \Phi_0 \exp[-\mu(\omega)x],$$



Fluorescence and Auger yields

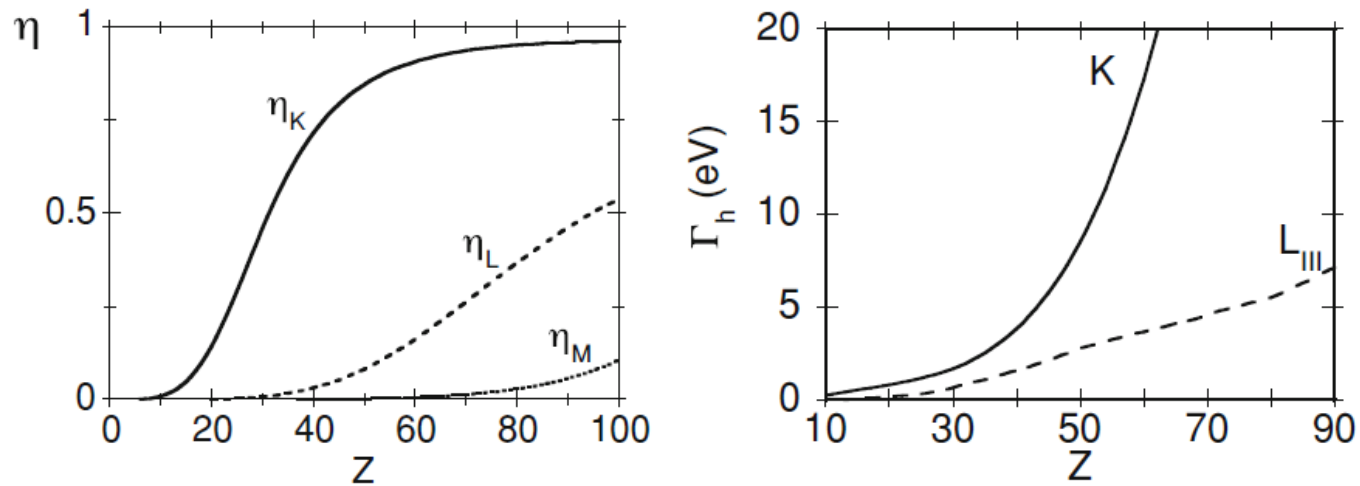


Fig. 6.4 Average fluorescence yield η (6.13) for the K, L and M edges (*left*) and width Γ_h of the K and L_{III} excited states (*right*) as a function of the atomic number Z

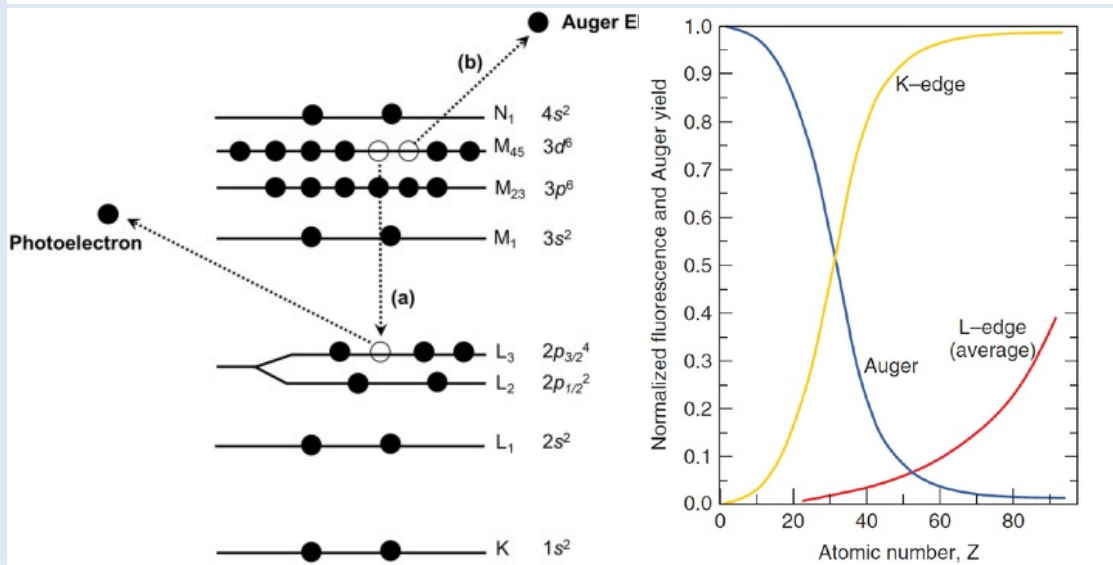
LBL/PUB-490 Rev. 3

Center for X-Ray Optics
and
Advanced Light Source

**X-RAY DATA
BOOKLET**

- | | |
|-------------------|-----------------|
| Albert Thompson | Ingolf Lindau |
| David Attwood | Yanwei Liu |
| Eric Gullikson | Piero Pianetta |
| Malcolm Howells | Arthur Robinson |
| Kwang-Je Kim | James Scofield |
| Janos Kirz | James Underwood |
| Jeffrey Kortright | Gwyn Williams |
| Herman Winick | |

October 2009



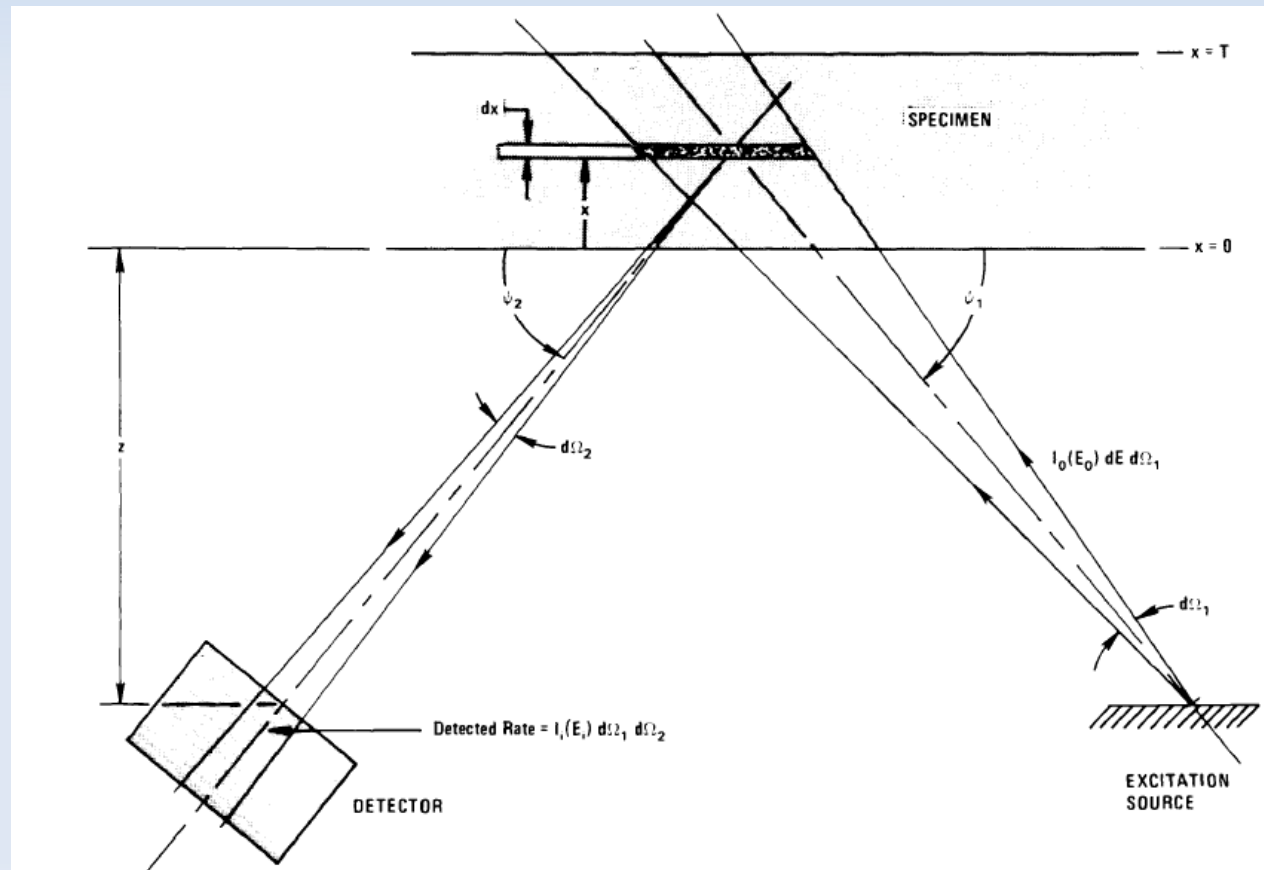
- Fluorescence de-excitation mechanisms largely prevail for K-edge hard x-ray absorption measurements. Auger and electron yield are used mainly for soft x-ray measurements

X-ray fluorescence

There are different methods for collecting XRF spectra depending on the particular experimental needs, basically divided into energy (EDX, EDS) and angular dispersive (WDX) techniques. Energy dispersive requires a solid-state detector and a multichannel electronics, angular dispersive a complex setup including monochromators for the emitted photons.

EDX is nowadays a standard at x-ray scanning-energy beamlines for collecting XRF signals of dilute samples.

- Energy resolution is limited (typically 130 eV or 120 eV FWHM for Si(Li) or Ge detectors, at 6 keV, increasing with $E^{1/2}$).
- Depending on the monochromator setup, very high resolutions can be achieved using WDX.

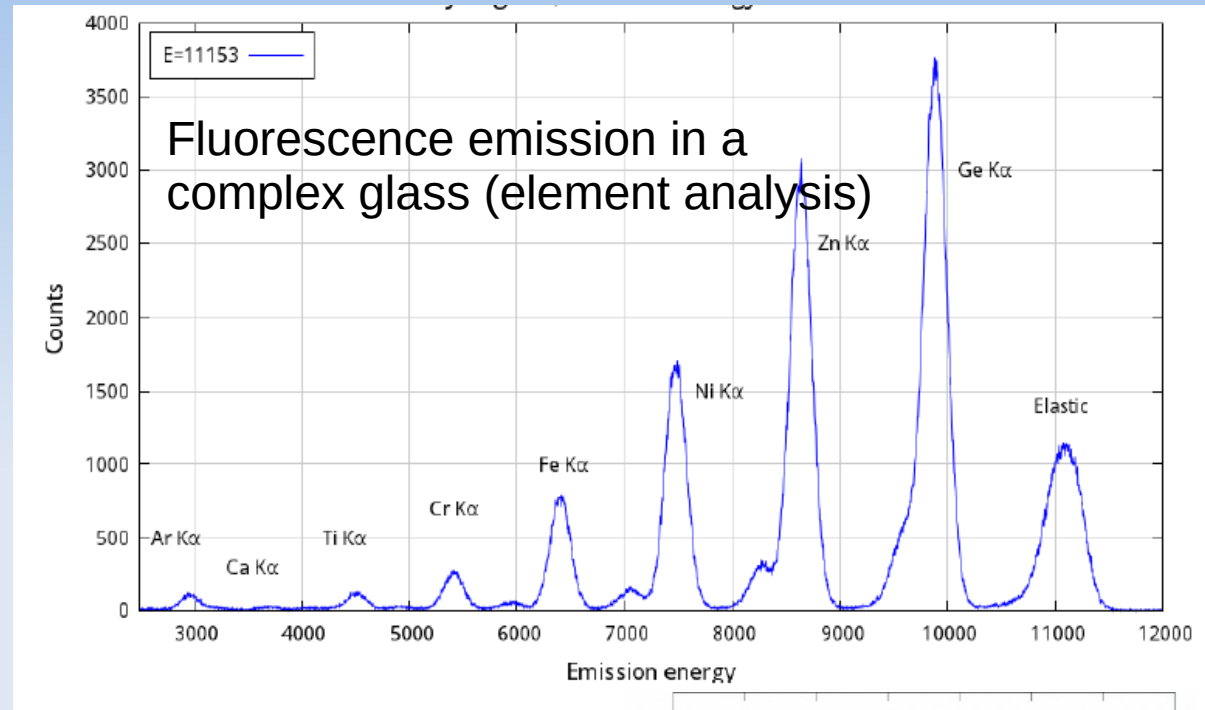


X-ray fluorescence

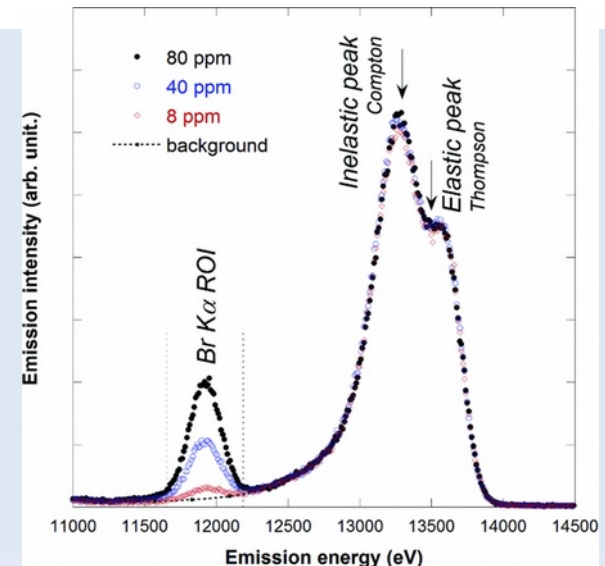
Mostly used in the hard x-ray regime, at synchrotrons for dilute atomic species/samples

High-tech solid-state detectors can improve collection statistics by increasing the collected solid angle (multi-element) and with a low-noise electronics (the selected „ROI” contains usually only a small portion of the signal)

* Precautions must be taken for thick samples (corrections for self-absorption and increased background, filters)

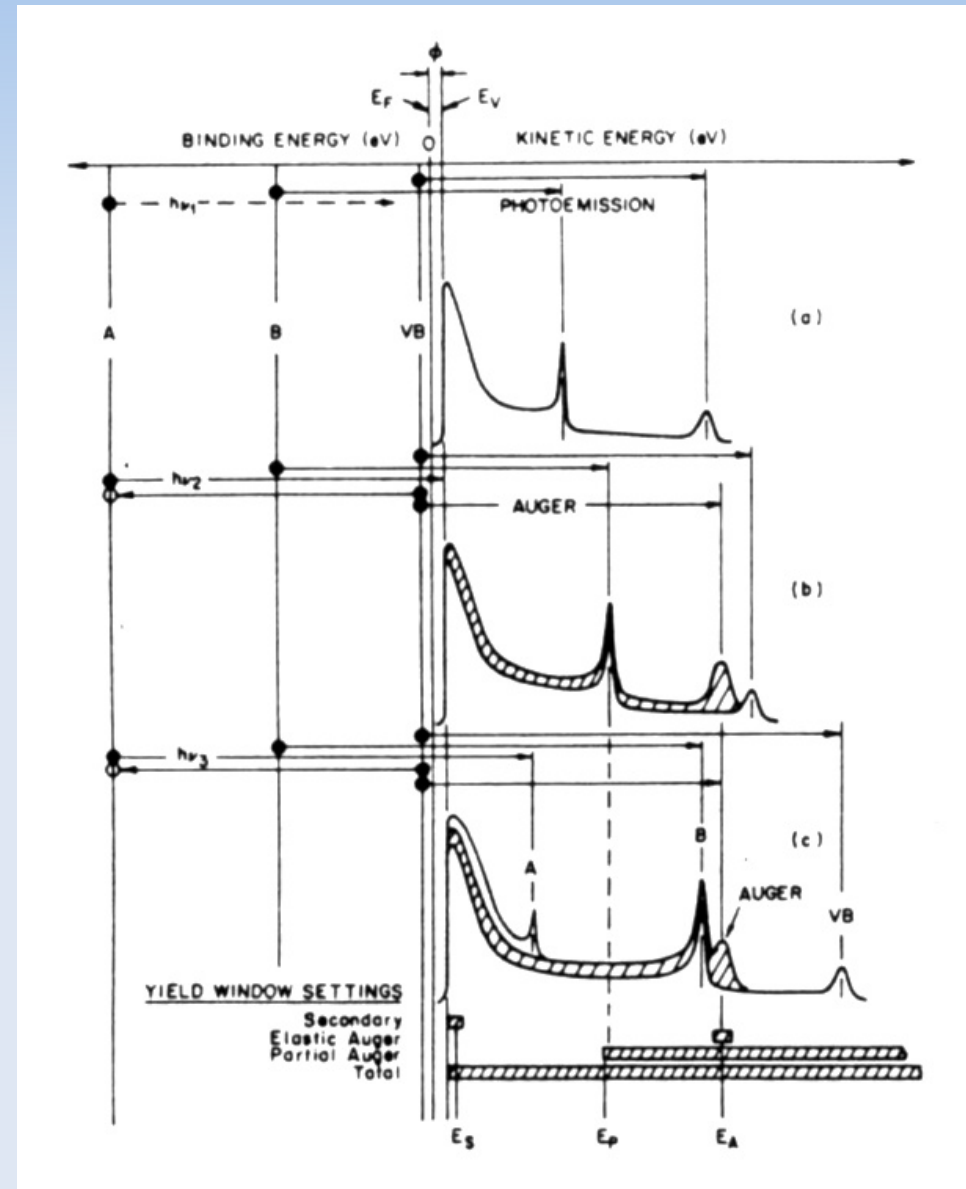


Fluorescence emission in Br solutions of increasing concentrations



Electron yield techniques

- Especially useful for in the soft x-ray range
- Surface sensitivity
- Different options for measuring x-ray absorption (Auger yield, total or partial yield)
- Usually needing high vacuum technology/conductive samples



X-ray Absorption Spectroscopy: synchrotron radiation experiments

XAS – X-ray Absorption Spectroscopy
XAFS – X-Ray Absorption Fine Structure
EXAFS – Extended XAFS

Transmission
mode

Transmission XAS

$\mu(E) = \ln(I_0/I_t)$, i.e. Beers' Law for X-rays

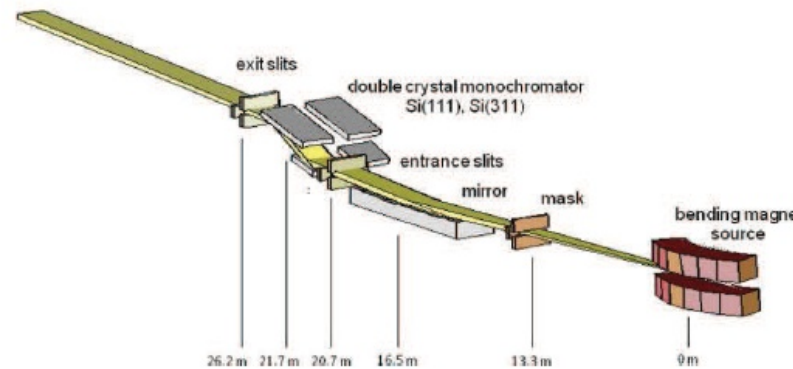
and/or
Photon-in,
photon-out
(fluorescence
mode)

Fluorescence XAS

$\mu(E) \propto I_f/I_0$

and/or
electron yields

+... *x-ray
diffraction/laser
beams*



Hard X-rays are deeply penetrating into matter, so the stage could be:

- Cryostat
- Furnace
- Pressure cell
- Electrochemistry cell
- Stop-flow cell
- Gas flow reactor

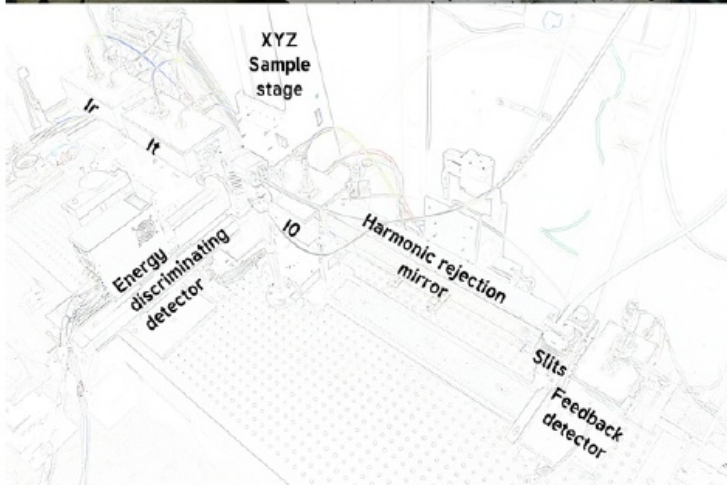
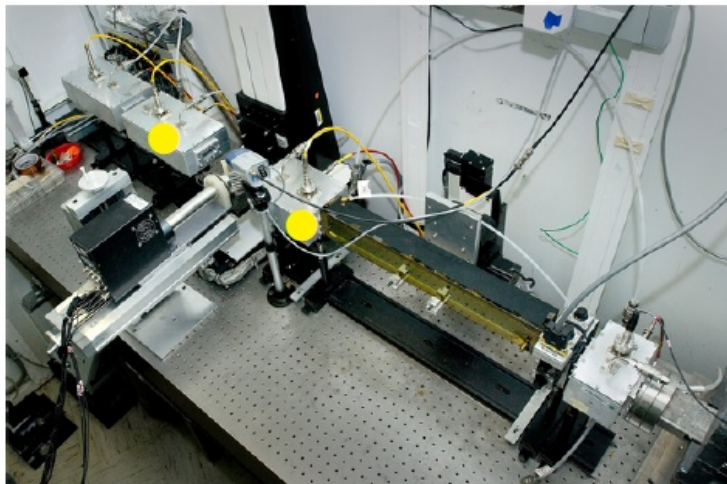
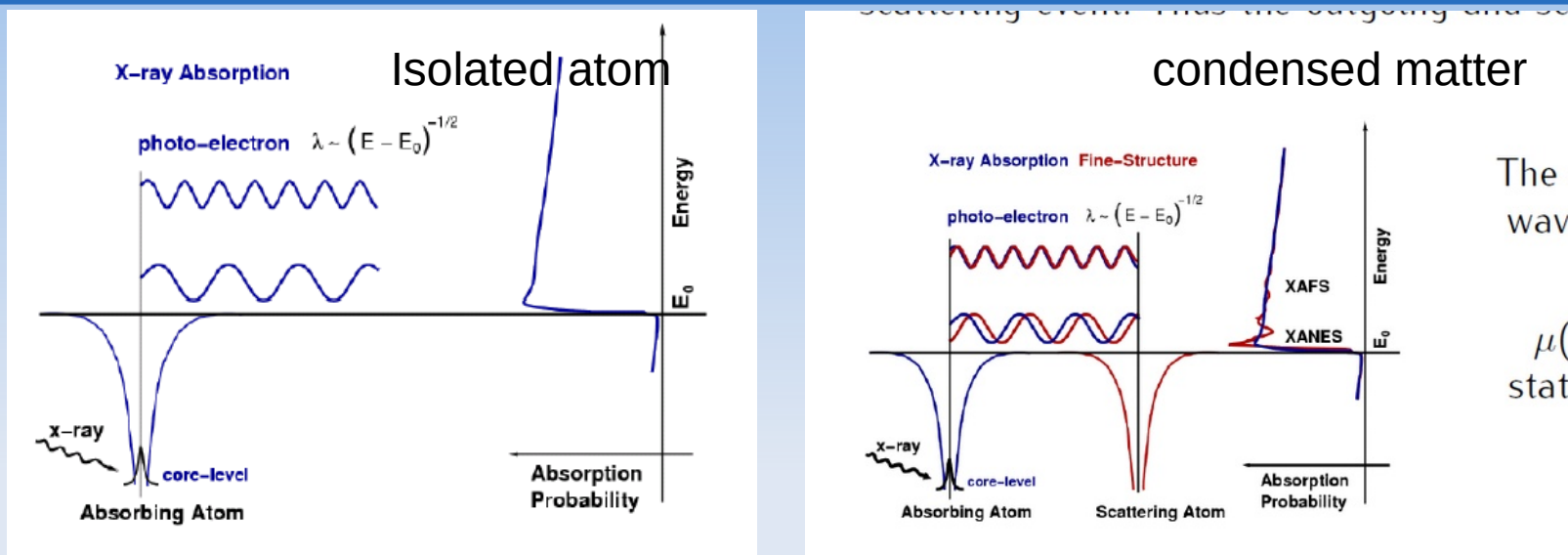


Photo is of the hutch from NLSL beamline X23A2

X-ray absorption: simple picture



The s
wave
 $\mu(l)$
state

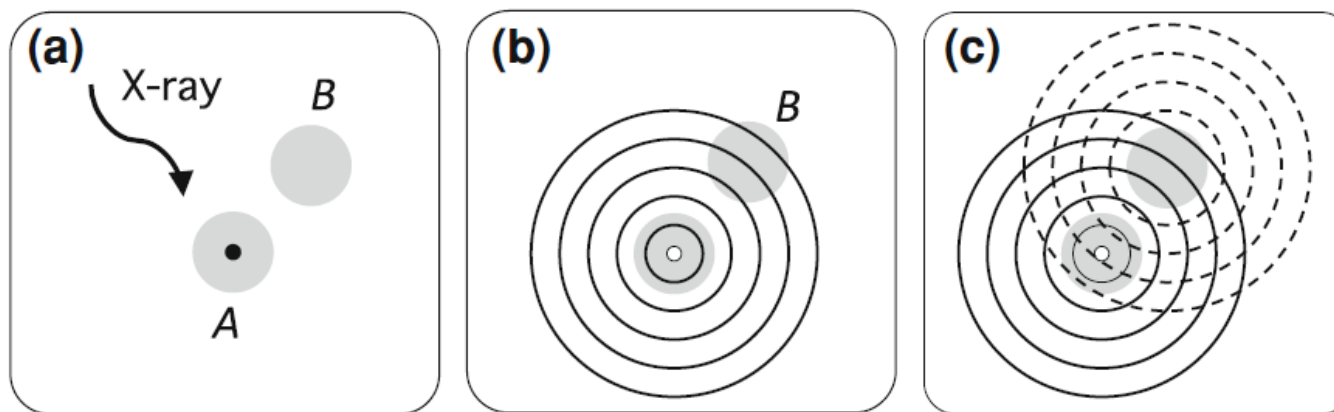
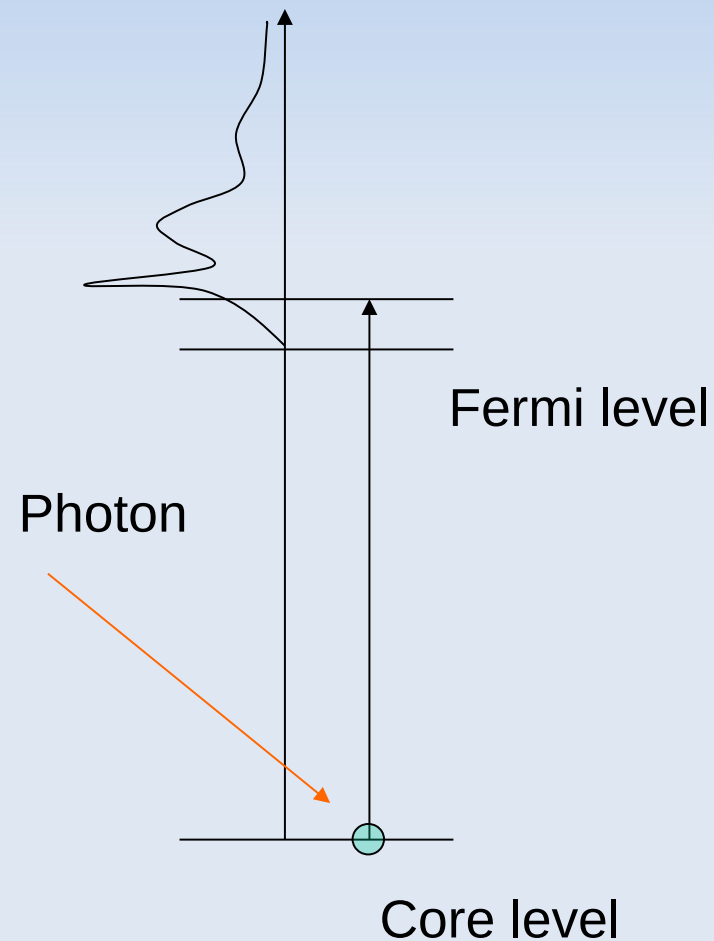
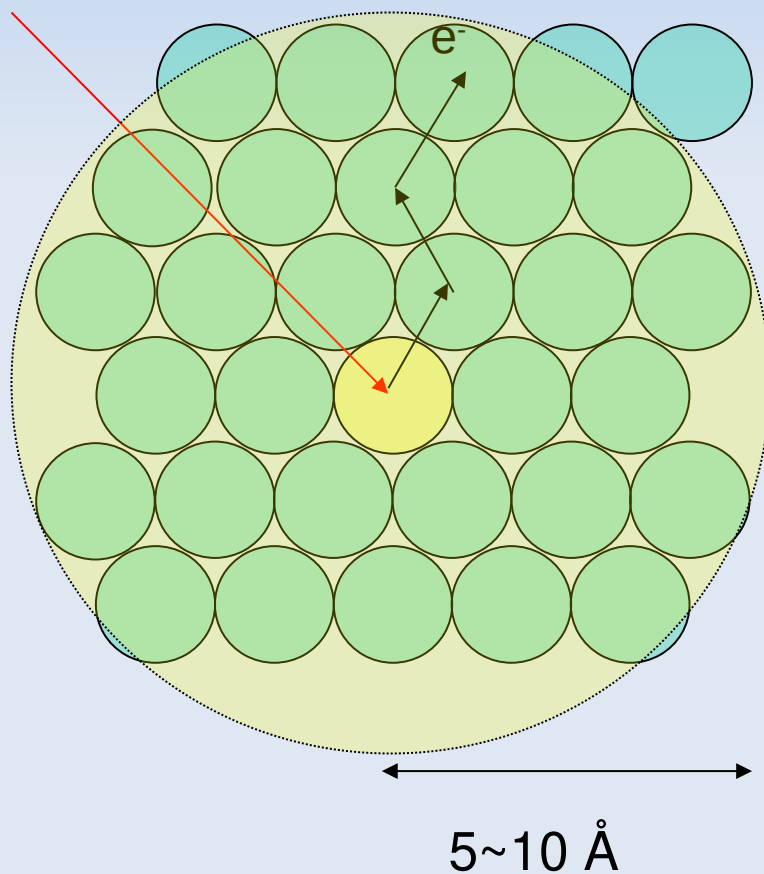


Fig. 6.3 Schematic picture of the EXAFS phenomenon: **a** the X-ray photon impinging on atom A (the *black circle* is the orbital of the core electron), **b** the outgoing photo-electron wave function (the *open circle* is the core hole of atom A), **c** the final state superposition of the two wavefunctions, outgoing from atom A and scattered from atom B

Core-electron Photo Absorption

The excited electron range is limited by the lifetime of the excited state. Thermalization of the highly excited electron is fast and interference processes are lost at long range

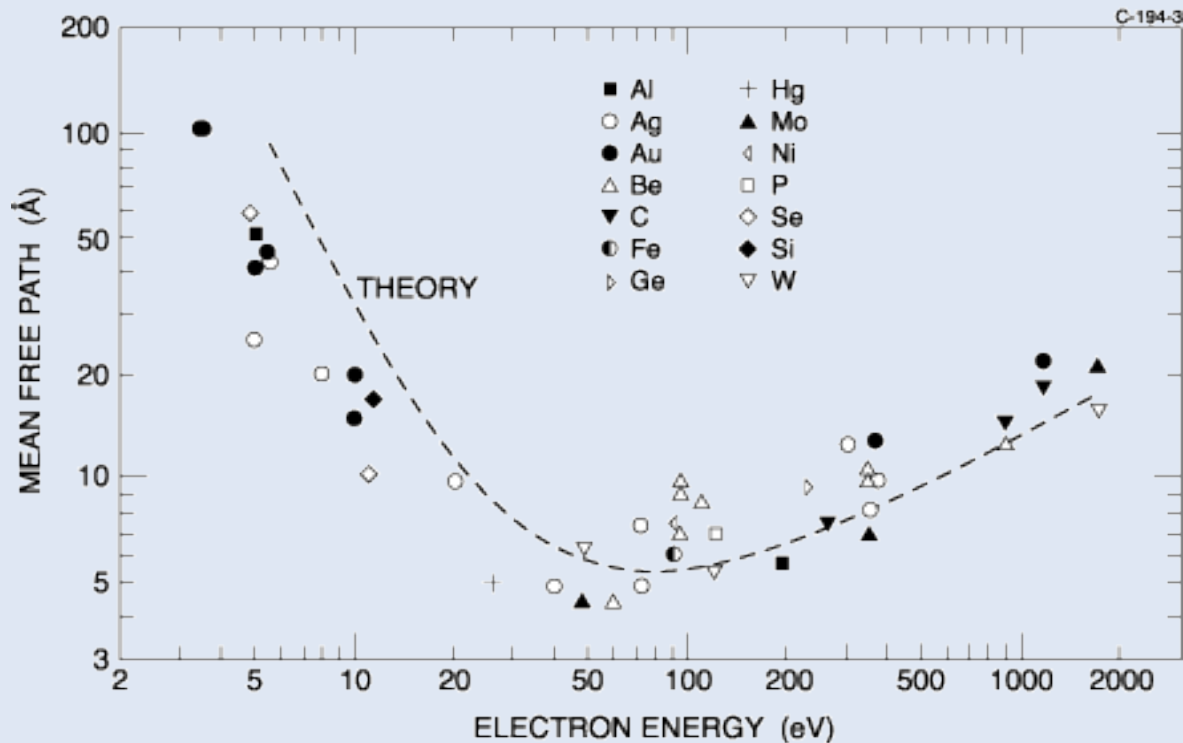
Photon



XAS – photon pump/electron probe

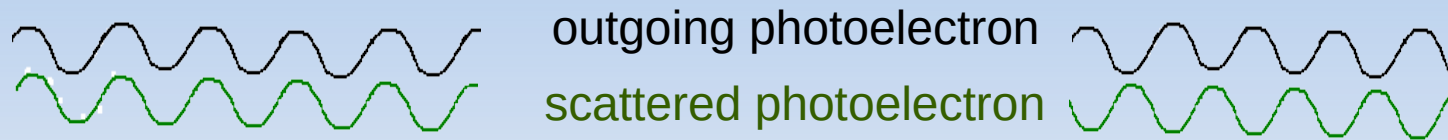
Due to the finite lifetime of core-hole and the mean free path of excited electron, we need to consider only a cluster in few Å size

→ EXAFS is sensitive to the local structure!

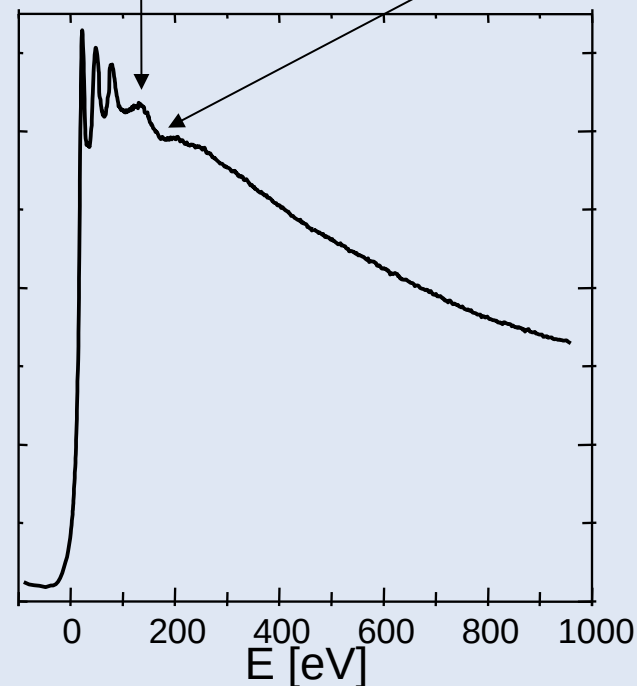


XAS interference effect

The absorption coefficient is affected by the interference processes contributing to the final photoelectron state, so information about the local structure can be derived looking at the modulation of the absorption signal



Constructive interference maximum Destructive interference minimum



The XAS structural signal

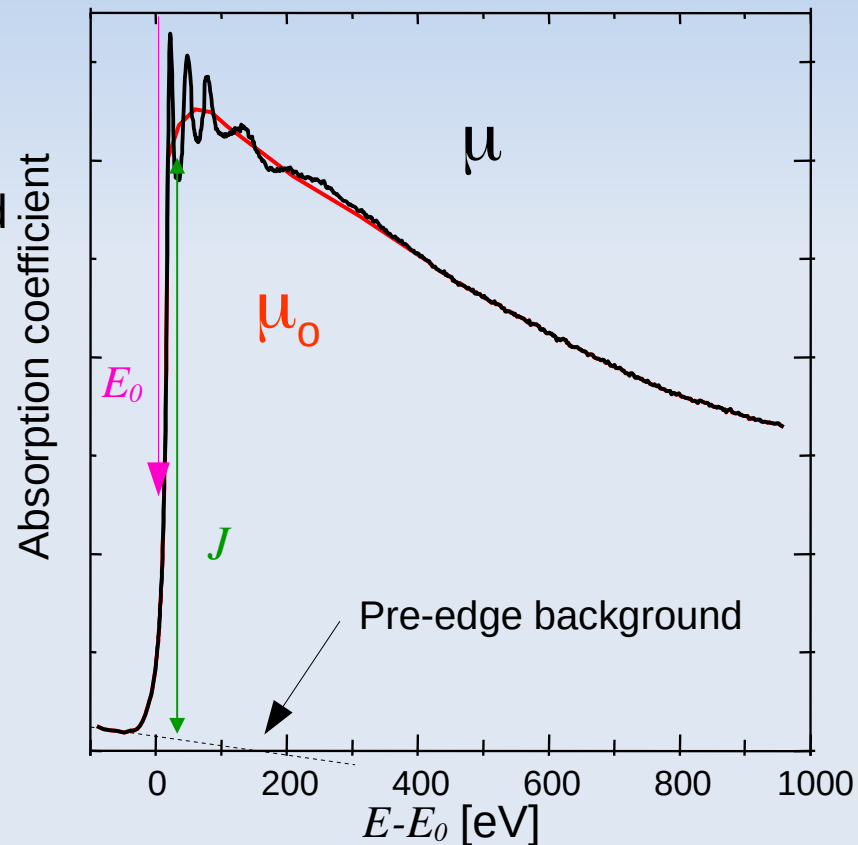
The XAS structural signal is the normalized modulation of the absorption coefficient

$$\chi(E) = \frac{\mu(E) - \mu_0(E)}{\mu_0(E)}$$

→ The absorption coefficient of the selected core level must be isolated removing the pre-edge background absorption and possible other smooth background contributions: $\mu(E) = \mu_{\text{expt}}(E) - b(E)$

→ The atomic absorption normalization can be approximated by cross-section calculations of $\sigma_0(E)$ (hydrogenic approximation for instance): $\mu_0(E) = J\sigma_0(E)$ here J is the absorption discontinuity at the edge $\Delta\mu(E_0)$

→ Sometimes the approximate form is used neglecting the energy dependence

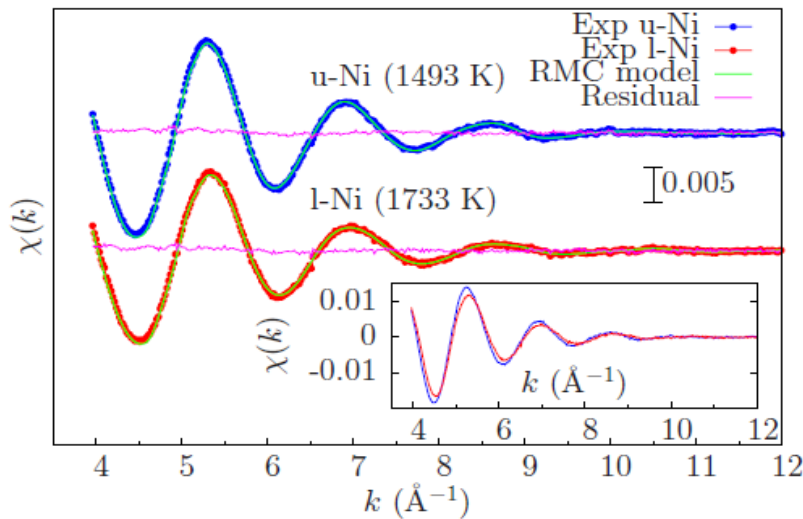


$$\chi(E) = \frac{\mu(E) - \mu_0(E)}{\Delta\mu_0(E_0)}$$

XAS (EXAFS) at a first glance

The XAS structural signal $\chi(k)$ is a regular oscillation as a function of the photoelectron wave-vector k :

$$k = \sqrt{[2m(E_{h\nu} - E_0)/\hbar^2]}$$



Pt L3-edge XAS of crystalline Pt and different nanocrystalline forms

Ni K-edge XAS of liquid Ni at different temperatures

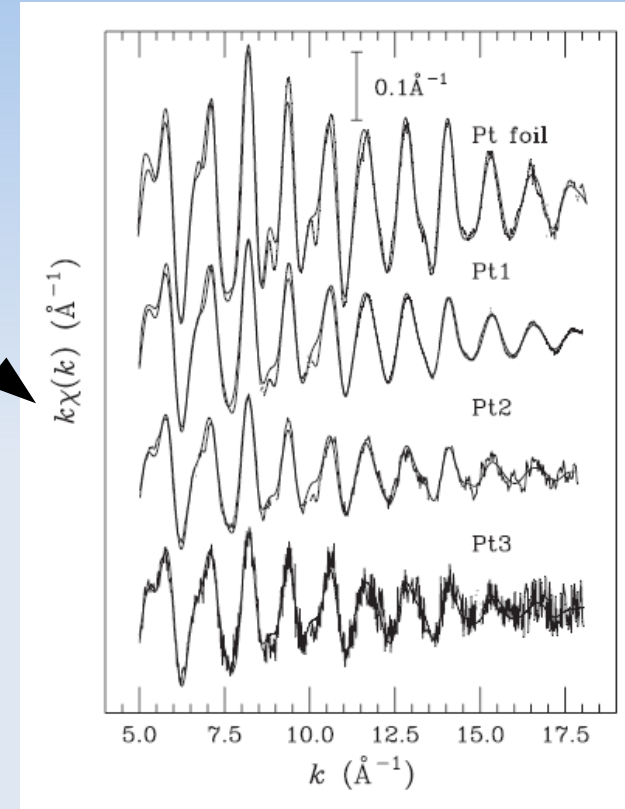


FIG. 2. Comparison of calculated (RMC simulation, green

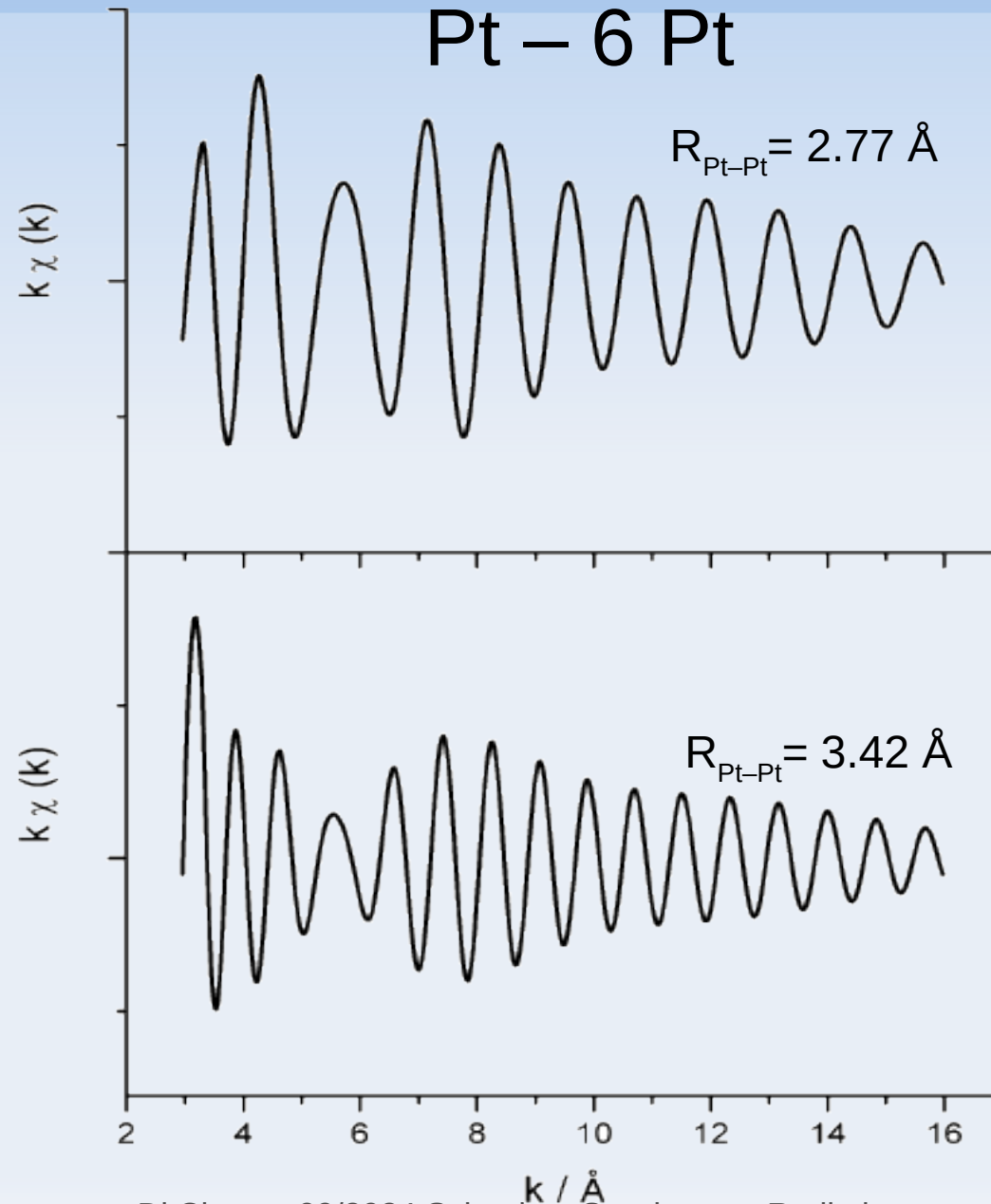
Standard EXAFS formula (oversimplified)

$$\chi(k) = \sum_j \frac{N_j S_0^2 f_j(k) e^{-2R_j/\lambda(k)} e^{-2k^2\sigma_j^2}}{kR_j^2} \sin[2kR_j + \delta_j(k)]$$

Example of XAS sensitivity (distances)

Main effect:
frequency change.

Higher frequency \rightarrow
longer interatomic
distances R

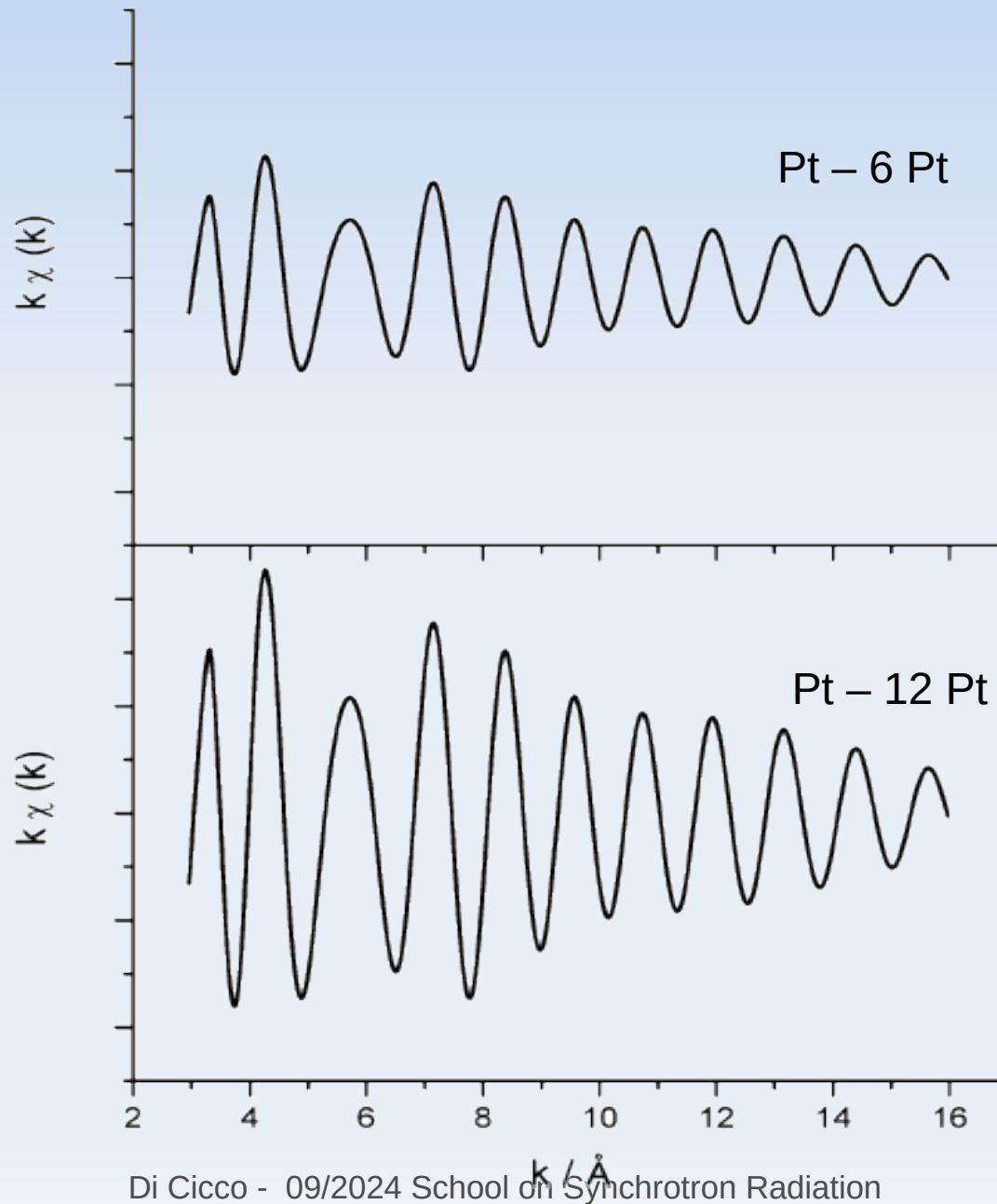


XAS sensitivity (number of neighbors)

Main effect: amplitude change.

The amplitude scales linearly with the number of neighbors (**N**)

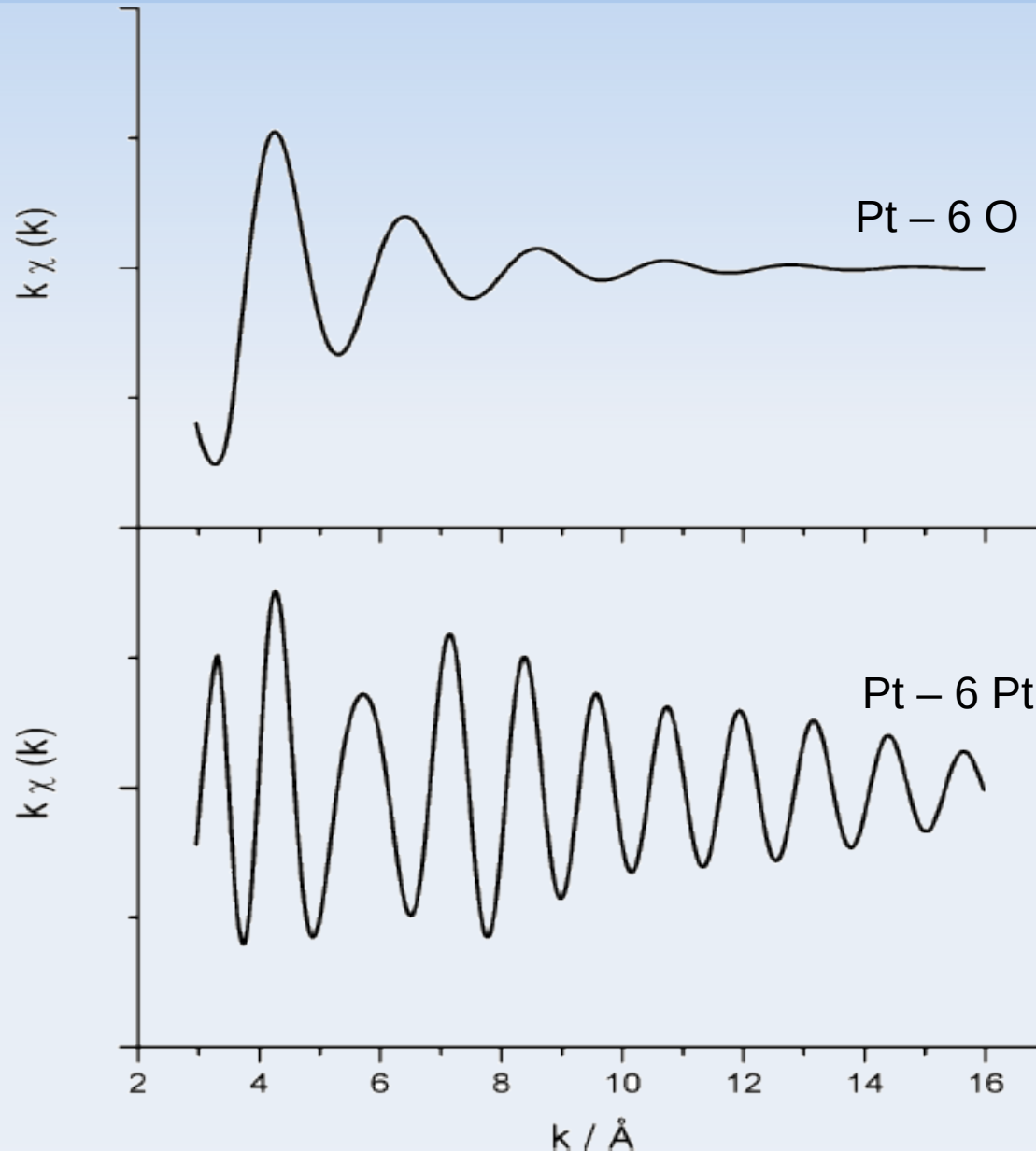
The amplitude of the signals is also exponentially damped in k^2 through a disorder factor (Debye-Waller Like)



Example of XAS sensitivity (chemistry)

Main effect: k-dependent amplitude change
Minor phase change effects are present too

The amplitude depends on the scattering power of the neighboring atoms (related roughly to the atomic number)



Interpretation of XAS

- Oscillations of the core level absorption cross-section for molecules and crystals known since about 100 years
- SRO and LRO theories used for interpretation for long time
- 70s: initial use of synchrotrons and application of a simple Fourier Transform method for XAS data-analysis: Sayers, Stern, Lytle, PRL 27, 1204 (1971)
- mid seventies: a real-space multiple-scattering approach is shown to be successful (Lee and Pendry PRB 8, 2795 (1975) ...)
- 80s-today: computer developments make it possible multiple-scattering (MS) data-analysis both for near-edge and EXAFS spectra
- Advanced main MS programs developed and currently available:
 - English school EXCURVE (Daresbury), J.Phys. C, 21, 3699 (1988).
 - US school FEFF (Seattle), PRB 44, 4146 (1991).
 - Italian school GNXAS (Frascati), SSC 78, 265, 1991; PRB 52, 15122, 1995

XAS: Current computational strategies and approximations

The x-ray absorption cross-section for a given excitation channel, indicating with α the fine structure constant and $\hbar\omega$ the photon energy, is expressed by:

$$\sigma(\hbar\omega) = 4\pi^2\alpha \hbar\omega \sum_f |\langle i|\hat{\epsilon} \cdot \vec{r}|f\rangle|^2 \delta(E_f - E_i - \hbar\omega) \quad (1)$$

Underlying approximations:

The photo-absorption process is dominated by dipole transitions;

It is a one-electron process: $|i\rangle$ and $|f\rangle$ are the initial (ground state) and final (excited state) 1-electron wave-functions;

$|f\rangle$ is calculated using an effective potential for the excited state

$$V(\vec{r}, E) = V_{\text{Coulomb}}(\vec{r}) + \Sigma(E, \rho(\vec{r}));$$

$\Sigma(E, \rho(\vec{r}))$ is the self-energy for an electron traveling in a uniform electron gas of density ρ , accounting approximately for exchange and correlation effects;

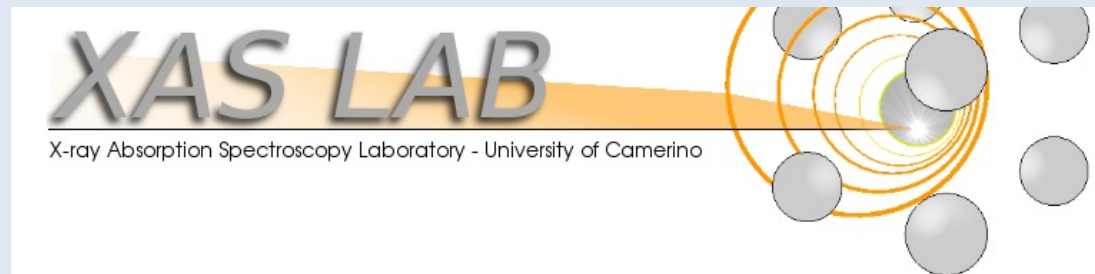
$V(\vec{r}, E) = \sum_j V_j(\vec{r} - \vec{R}_j)$ is approximated by a decomposition of spherically symmetrical contributions V_j centered around each atomic site, embedded into a constant potential;

As a result of the previous Muffin-tin approximation, $|f\rangle$, or more conveniently the Green's function $G^+(E)$ for the final state Hamiltonian, can be computed as a result of a scattering process of a photo-electron wave over the surrounding spherically symmetric potentials.

$$\sigma(\hbar\omega) = 4\pi^2\alpha \hbar\omega \frac{1}{\pi} \text{Im} \langle i|\hat{\epsilon}^* \cdot \vec{r}'|G^+(E_i + \hbar\omega)|\hat{\epsilon} \cdot \vec{r}|i\rangle \quad (2)$$

GnXAS collaboration

- *Main GnXAS development (1990-1996): A. Filipponi A. Di Cicco and C. Natoli*
- *Collaborators contributing also to previous GnXAS workshops and schools (1992-2022) P. D'Angelo, K. Hatada, F. Iesari, M. Minicucci, E. Principi, A. Trapananti, A. Witkowska ...*
- *The Camerino XAS group is currently distributing GnXAS to the scientific community. Its use is recommended under Linux operative system, but it can be adapted to MAC OsX and Windows (K. Hatada, F. Iesari).*
- *Longstanding scientific activity in the last 35 years on XAS under non-standard conditions carried out at ADONE (Frascati), LURE (Orsay) and since 1995 at the ESRF (Grenoble), since 2006 ELETTRA (Trieste), since 2007 at Soleil (Saclay).*
- <http://gnxas.unicam.it> Website



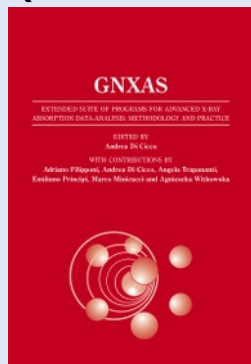
Documentation

Guidelines for installation and usage are available at the website <http://gnxas.unicam.it>

Free downloading of executables and updated 2023 version


Data analysis examples

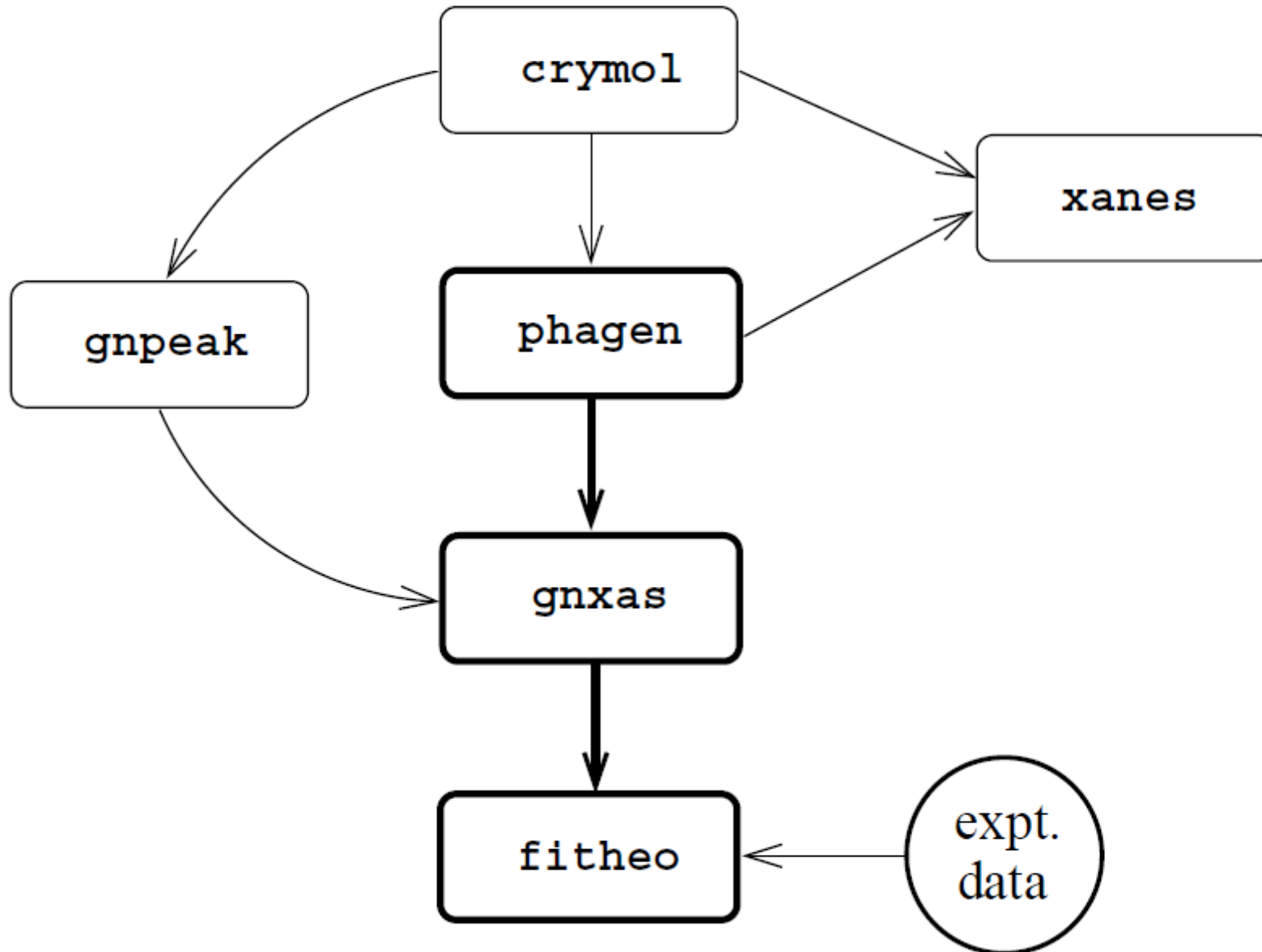
Full documentation on GNXAS and related programs available (GnXAS red book 2009)



The screenshot shows the GNXAS website homepage. At the top, there is a header with the XAS LAB logo (University of Camerino), the School of Science and Technology Physics Division logo, and a stylized atomic model. The main content area is divided into a left sidebar and a main right section. The sidebar contains navigation links: HOME, RESEARCH, TEACHING, GNXAS, Publications and Highlights, Press and Awards, Life of the group, and Links. Below the links is a yellow 'USE CAUTION' sign with a hand near a sharp edge and the text 'NEAR THE EDGE FOOTING CAN BE DANGEROUS'. The main section is titled 'GNXAS' and features a 'Current versions: 11.2013/12.2006' notice. It lists several links: GNXAS info and news, Introduction to GNXAS, Program Description, Documentation GNXAS 'red-book', Who wrote GNXAS, and Where to find GNXAS. Below this is an 'Info and News' section with links to latest intensive courses and news. A 'Become a GNXAS user in 5 steps' section follows, listing steps from downloading to data analysis examples. An 'Info about all the GNXAS distributions' section lists various versions and their dates. A 'DOCUMENTATION' section includes a link to the full and updated GNXAS documentation (2009) 'red-book' and a thumbnail of the book cover. An alternative link to 'TASK QUARTERLY' is also provided.

GNXAS data-analysis

 Flow diagram of the GNXAS package



The x-ray absorption cross-section: dipole approximation

$$(7) \quad \sigma(\hbar\omega) = 4\pi^2 \alpha \hbar\omega \sum_f |\langle i | \vec{\epsilon} \mathbf{r} | f \rangle|^2 \delta(E_f - E_0 - \hbar\omega)$$

where $\alpha = e^2 / \hbar c \sim 1/137$ is the fine structure constant.

This equation is written within a simple one-electron scheme where there is only one charge interacting with the field. In a many-body approach $|i\rangle$ and $|f\rangle$ are the initial and final many-electron wave functions and the dipole operator contains all of the possible electron coordinates $\vec{\epsilon} \sum_i \mathbf{r}_i$.

The wave function of the initial state can be separated in angular and radial parts:

$$(8) \quad |i\rangle = Y_{l_0, m_0}(\hat{\mathbf{r}}) R_{l_0}^0(r)$$

l_0 is the angular momentum of the electron and Y_{l_0, m_0} are the spherical harmonics functions, solution of the angular part of the Schrödinger equation.

The final state after photo-excitation is a wave traveling in the medium of well-defined energy E and wave-vector \mathbf{q} and can be also expanded

$$(9) \quad |f\rangle = \sum_{l, m} C_{l, m} Y_{l, m}(\hat{\mathbf{r}}) R_q(r)$$

in “partial” waves of selected angular momentum.

Dipole selection rules

The dipole term can be also expressed in term of spherical harmonics and dipolar selection Rules are obtained in the matrix element ($l_0 \rightarrow l_0-1, l_0 \rightarrow l_0+1$ only channels allowed).

$$Y_{1,0} = \sqrt{\frac{3}{4\pi}} \cos\theta$$

$$(11) \quad Y_{1,\pm 1} = \mp i \sqrt{\frac{3}{8\pi}} \sin\theta e^{i\phi}$$

we obtain a simple expression:

$$(12) \quad \vec{e}_r = r \sqrt{\frac{4\pi}{3}} Y_{1,m_\gamma}$$

where $m_\gamma = 0, 1, -1$ corresponds to linear, right and left circular polarizations respectively.

For unpolarized radiation or when the sample does not show preferential directions (crystalline powders or disordered systems) we can write a polarization-averaged matrix element:

$$(13) \quad |\langle f | \vec{e}_r | i \rangle|^2 = \frac{1}{3} \sum_{m_\gamma} |\langle f | r Y_{1,m_\gamma} | i \rangle|^2 \frac{4\pi}{3}$$

A great simplification is obtained by separating angular and radial coordinates in the integration of the matrix element. The well-known dipolar **selection rules** are obtained by the following equation involving spherical harmonics:

$$(14) \quad \sum_{m_0, m_\gamma} \langle Y_{l,m} | Y_{l_0, m_0} Y_{1, m_\gamma} \rangle \langle Y_{l_0, m_0} Y_{1, m_\gamma} | Y_{l', m'} \rangle$$

$$= \frac{3}{4} \delta_{l, l'} \delta_{m, m'} \left[\frac{l_0}{2l+1} \delta_{l, l_0-1} + \frac{l_0+1}{2l+1} \delta_{l, l_0+1} \right]$$

XAS cross-section: spherical atom

The x-ray absorption cross-section for transitions of a s core-electron to continuum states can be written as:

$$\begin{aligned} \sigma(\hbar\omega)_{K,L_I\dots} &= 2 \cdot 4\pi^2 \alpha \hbar\omega \frac{1}{3} \sum_{m_\gamma} \sum_m \left[\frac{l_0 + 1}{2l_0 + 1} \delta_{l,l_0+1} |M_{l_0,l_0+1}|^2 \right]_{l_0=0} \\ (16) \qquad \qquad \qquad &= \frac{8}{3} \pi^2 \alpha \hbar\omega |M_{l_0,l_0+1}|^2 \end{aligned}$$

where we have taken into account **the spin degeneracy (2)** and the **polarization average**. For hydrogen the matrix element can be solved exactly using the continuum wave functions:

$$(17) \qquad |R_{l=1,E_f} r^3 R_{n=1,l=0}|^2 = \frac{2^8}{Z^4} \frac{a_0^3}{e^2} \left(\frac{\eta^2}{1 + \eta^2} \right)^5 f(\eta)$$

where $\eta = \sqrt{\frac{E_0}{\hbar\omega - E_0}}$ and $f(\eta) = \frac{e^{-4\eta \arccot \eta}}{1 - e^{-2\pi\eta}}$.

Thus the cross-section becomes:

$$(18) \qquad \sigma(\hbar\omega)_{K,L_I\dots} = \frac{8}{3} \pi^2 \alpha \hbar\omega \frac{2^8}{Z^4} \frac{a_0^3}{e^2} \left(\frac{\eta^2}{1 + \eta^2} \right)^5 f(\eta)$$

1-atom scattering theory

Free particle S. equation ($V(r) = 0$):

$$(19) \quad \hat{H}\Psi = \frac{-\hbar^2}{2m} \Delta\Psi = E\Psi$$

A possible solution is $\Psi = \sum_{l,m} A_{l,m} R_l(r) Y_{l,m}(\hat{r})$ where $Y_{l,m}$ are the spherical harmonics (angular coordinates), and R_l is composed of Bessel j_l and Neumann n_l functions defined as:

$$(20) \quad j_l(kr) = (-1)^l \frac{r^l}{k^l} \left(\frac{d}{r dr} \right)^l \frac{\sin(kr)}{kr}$$

Those functions (Neumann's are obtained using $\cos(kr)$ instead of $\sin(kr)$) are solution of the radial equation:

$$(21) \quad \left[\frac{d^2}{d\xi^2} + \frac{2}{\xi} \frac{d}{d\xi} + 1 - \frac{l(l+1)}{\xi^2} \right] R_l(r) = 0$$

where $\xi = kr$.

The asymptotic behavior for $\xi \rightarrow \infty$ is:

$$(22) \quad j_l(kr) \sim \frac{1}{kr} \sin \left(kr - l \frac{\pi}{2} \right)$$

Muffin-tin

If we switch on the potential in a finite spherical region $r < R_{MT}$ we can write the equation:

$$(23) \quad \left[\frac{d^2}{dr^2} + \frac{2}{r} \frac{d}{d\xi} + k^2 - \frac{l(l+1)}{r^2} - V(r) \right] R_l^{(+)}(r) = 0$$

where $V(r) = \frac{2m}{\hbar^2} U(r), r \leq R_{MT}$, and $V(r) = 0, r > R_{MT}$.

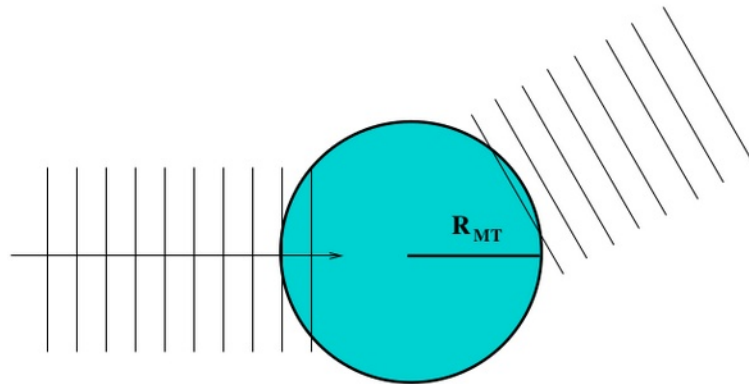


Figure 1: Sketch of the scattering process

The scattering potential of each atom is assumed to be spherically symmetric and limited in range: $V(r)=0, r>R_{MT}$

Wave function for a MT potential

A suitable combination of Bessel and Neumann functions will represent the wave-function for $r > R_{MT}$. However, the free-particle solution will depend on the interaction (potential energy) inside the sphere because the wave-function is continuous and derivable in the whole space.

Useful functions describing outgoing particles in free space interacting with spherical potentials are: $h_l^+(kr) = j_l(kr) + in_l(kr)$ (Hankel functions).

The (radial) solution for $r > R_{MT}$ can be written in the form:

$$(24) \quad R_l(kr) = j_l(kr) + it_l h_l^+(kr)$$

while in the region $r \leq R_{MT}$ we can solve the S. equation:

$$(25) \quad R_l(kr) = C_l R_l^0(r)$$

By imposing the continuity of the function and its first derivative we obtain:

$$(26) \quad C_l R_l^0(R_{MT}) = j_l(kR_{MT}) + it_l h_l^+(kR_{MT})$$

$$(27) \quad C_l R_l^0'(R_{MT}) = k \left[j_l'(kR_{MT}) + it_l h_l^+'(kR_{MT}) \right]$$

Definition of the t_l 's

Dividing the two equations we have ($R_{MT} = R$):

$$(28) \quad \frac{R_l^0{}'(R)}{R_l^0(R)} = \frac{k \left[j_l'(kR_{MT}) + it_l h_l^+{}'(kR_{MT}) \right]}{j_l(kR_{MT}) + it_l h_l^+(kR_{MT})}$$

Therefore we obtain:

$$(29) \quad t_l = i \frac{W[j_l, R_l^0]}{W[h_l^+, R_l^0]}$$

where we used the Wronskian $W[f, g] = fg' - gf'$.

The normalization factor C_l can be found by continuity:

$$(30) \quad C_l R_l^0(R_{MT}) = j_l(kR_{MT}) + it_l h_l^+(kR_{MT})$$

It can be shown that C_l is simply proportional to t_l and therefore the solution of the Schrödinger equation inside the sphere ($r < R_{MT}$) can be normalized in such a way that:

$$(31) \quad \begin{aligned} R_l(r) &= t_l \underline{R}_l^0(R_{MT}) & r \leq R_{MT} \\ R_l(r) &= j_l(kR_{MT}) + it_l h_l^+(kR_{MT}) & r > R_{MT} \end{aligned}$$

Relationship with phase-shifts

By its definition t_l represents the amplitude of the wave scattered from the potential and must satisfy $|t_l| \leq 1$. The scattering amplitude can be then written as $t_l = e^{i\delta_l} \sin\delta_l$ (with the important property $|t_l|^2 = \text{Im}t_l$).

The asymptotic behavior ($r \rightarrow \infty$) of the solution $R_l(r)$ in presence of the potential can be derived by that of j_l and n_l functions:

$$(32) \quad R_l(r) \sim e^{i\delta_l} \frac{1}{kr} \sin \left(kr - l\frac{\pi}{2} + \delta_l \right)$$

The δ_l functions are called “phase-shifts” and represent the phase difference between the asymptotic solution *in presence of the interaction potential $V(r)$* and that of the free particle. The δ_l functions (defined within 2π) are directly related to the potential (attractive field: $\delta_l > 0$).

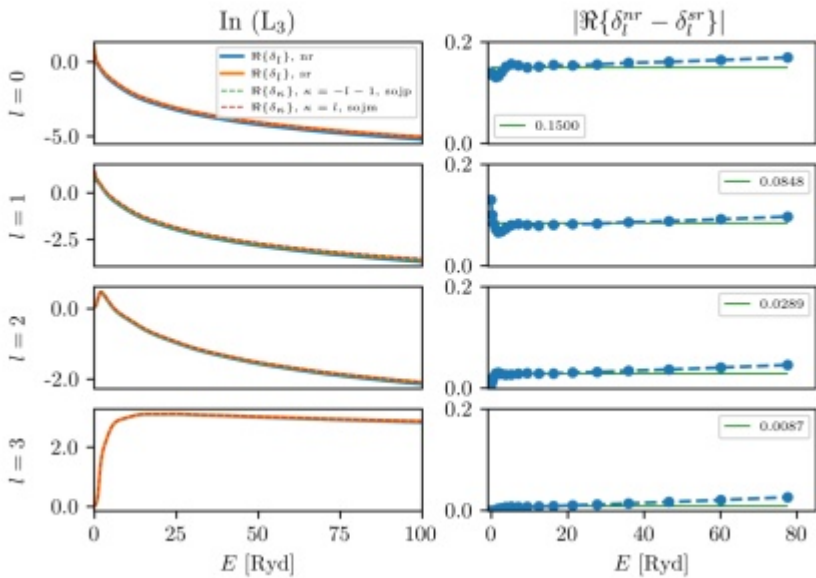
The usefulness of the partial wave expansion is related to its *convergence properties*. The number of l terms to be considered depends on the range of the potential.

A semiclassical argument is useful to explain this property: the angular momentum of a particle with momentum $p = \hbar k$ is $l = \hbar k s$ where s is the minimum distance from the scattering center. If the range of the potential is limited than $s \leq R$ and therefore only partial waves with $\frac{l}{\hbar} \leq kR$ have to be considered.

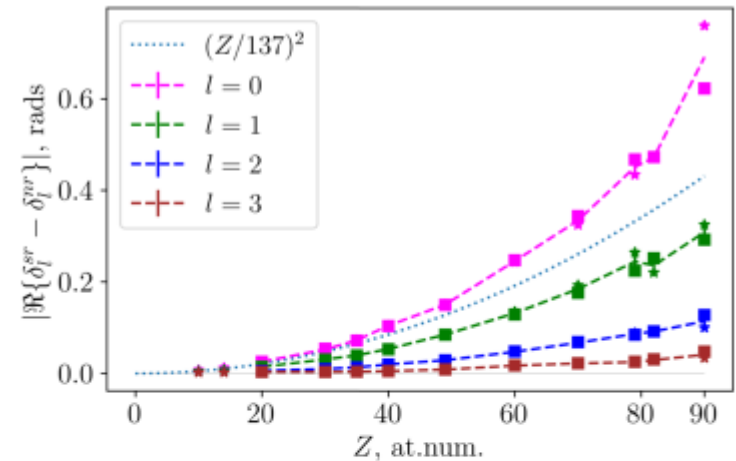
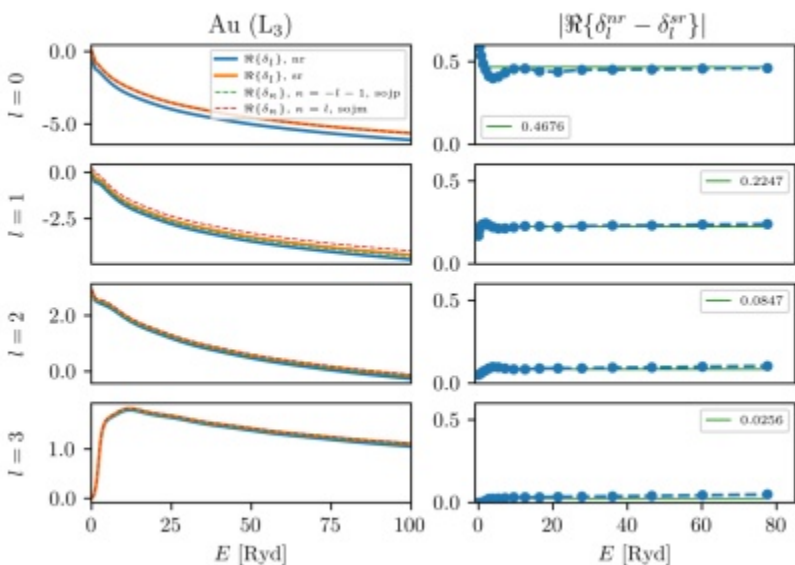
This result is confirmed also by more accurate quantum theory calculations and holds for finite range potentials and energies far from resonances.

Example of phase-shifts

In (Z=49) in body-centered-tetragonal crystalline



Au (Z=79) in fcc crystalline



K-edge (points with star)

L₃ edge (points with square)

The importance for relativistic effects in high-Z elements!

Phase-shifts at high kinetic energies for different angular momenta and increasing Z number.

[2]G. Tchoudinov, A. Di Cicco, and C. R. Natoli *Phys. Rev. B*, 105, 14410, 2022.

Scattering amplitude and cross-section

For a generic channel (initial angular momentum l_c) the x-ray absorption cross-section can be written as:

$$(33) \quad \sigma(\hbar\omega) = \frac{8}{3}\pi^2\alpha\hbar\omega [(l_c + 1)|M_{l_c, l_c+1}|^2 + l_c|M_{l_c, l_c-1}|^2]$$

where

$$(34) \quad M_{l_c, l} = \int_0^{R_{MT}} C_l R_l^{0*} R_{l_c} r^3 dr = t_l \int_0^{R_{MT}} \underline{R}_l^{0*} R_{l_c} r^3 dr$$

and by defining

$$(35) \quad |M_{l_c, l}|^2 = |t_l|^2 |M_{l_c, l}^0|^2$$

we obtain that the scattering amplitude is included directly in the cross-section

$$(36) \quad \sigma(\hbar\omega) = \frac{8}{3}\pi^2\alpha\hbar\omega [(l_c + 1)|t_{l_c+1}|^2 |M_{l_c, l_c+1}^0|^2 + l_c |t_{l_c-1}|^2 |M_{l_c, l_c-1}^0|^2]$$

Generalization for a collection of spherical potentials

It is possible to find a solution for the wave-function of an excited electron in an ensemble of spherical potential. Usually the problem is tackled using the Green function formalism (derivation shown in Faulkner and Stocks, PRB 21 1980, and more recently C. Brouder, D. Cabaret - Ph.D thesis).

In this context the "scattering path operators" plays the same role of the t_l but including all the multiple scattering events within the set of optical potentials. The scattering path operator is a matrix including both scattering amplitudes (T) and site-to-site propagators (G):

$$(37) \quad \tau_{L,L'}^{i,j} = [T^{-1} - G]^{-1} |_{L,L'}^{i,j} = T [1 - GT]^{-1} |_{L,L'}^{i,j}$$

The cross-section can be written as:

$$(38) \quad \sigma(\hbar\omega) = \frac{8}{3} \pi^2 \alpha \hbar \omega \left[(l_c + 1) \delta_{l,l_c+1} \Im M_{l_c,l}^{0*} \tau_{L,L}^{0,0} M_{l,l_c}^0 + l_c \delta_{l,l_c-1} \Im M_{l_c,l}^{0*} \tau_{L,L}^{0,0} M_{l,l_c}^0 \right]$$

where the atomic cross-section ($G = 0$) and the structural term are separated:

$$(39) \quad \sigma(\hbar\omega)_{0}^{l_c \pm 1} = \frac{8}{3} \pi^2 \alpha \hbar \omega |M_{l_c,l_c \pm 1}^0|^2 \Im T_{l_c,l_c \pm 1}^{0,0} = \frac{8}{3} \pi^2 \alpha \hbar \omega |M_{l_c,l_c \pm 1}^0|^2 \sin^2 \delta_{(l_c \pm 1)}$$

Cross-section for a collection of MTs

The structural term is defined as:

$$(40) \quad \chi(\omega)_0^{l_c \pm 1} = \left[\Im \frac{1}{\Im(t_0^{l_c \pm 1})} \frac{1}{2(l_c \pm 1) + 1} \sum_m [T(I - GT)^{-1}]_{0,0}^{l_c \pm 1, l_c \pm 1, m, m} \right].$$

and the cross section becomes

$$(41) \quad \sigma(\hbar\omega) = (l_c + 1)\sigma_0^{l_c + 1} \chi(\omega)_0^{l_c + 1} + (l_c)\sigma_0^{l_c - 1} \chi(\omega)_0^{l_c - 1}$$

Within this formalism the cross-section for the excitation of an electron within a collection of spherical atoms is obtained by the simple atomic cross section σ_0 just substituting the scattering amplitude t with the matrix element scattering path operator τ calculated on the photoabsorbing site (where the overlap between the core wave function and the wave function of the excited electron is not negligible).

Modeling x-ray absorption using the MS theory

The polarization averaged XAS cross-section for transitions to a dipole selected final state of angular momentum l_0 can be written as

$$(42) \quad \sigma(\omega) = \sigma_0 \left[\Im \frac{1}{\Im(t_0^{l_0})} \frac{1}{2l_0 + 1} \sum_{m_0} [T(I - GT)^{-1}]_{0,0}^{L_0, L_0} \right].$$

Here σ_0 is the atomic cross-section, T and G are the atomic scattering and propagator matrices in a local basis, indexed by i, j running over the different atoms, and by a set of angular momenta L, L' (where $L = \{l, m\}$).

The T scattering matrix here is block diagonal ($T_{i,j} = t_i \delta_{i,j}$) and, in the MT approximation for the potential, also diagonal on the the L indices ($t_i^{L,L'} = t_i^L \delta_{L,L'}$).

$$(43) \quad T = t_i \delta_{i,j} \delta_{l,l'} \delta_{m,m'}$$

In terms of the l -th potential phase shift: $t_i^l = \exp(i\delta_i^l) \sin(\delta_i^l)$.

T matrix elements are calculated by solving the Schrödinger equation for the potential at the corresponding i site.

Remark: all MS equations, and in particular the XAS cross-section, remains unaltered if one replaces the MT spheres with space filling cells (no interstitial region), but t^l is replaced by $t^{L,L'}$, taking in this way into account the non spherical shape of the cell potential (non MT potentials).

A. Filipponi, A. Di Cicco and C. R. Natoli, Phys. Rev. B 52, 15122 (1995)

Geometry probed by propagators

The propagator matrix is composed of null diagonal blocks, (i, i) sites, and non null off-diagonal blocks $G_{i,j}^{L,L'}$ describing the free propagation from site i to site j ($i \neq j$). The expression for a single propagator block involves 3J symbols and is given by:

$$(44) \quad G_{i,j}^{L,L'} = [4\pi(2l+1)(2l'+1)]^{\frac{1}{2}} \sum_{l_1} (2l_1+1)^{\frac{1}{2}} \begin{pmatrix} l & l' & l_1 \\ 0 & 0 & 0 \end{pmatrix} \begin{pmatrix} l & l' & l_1 \\ m & -m' & m' - m \end{pmatrix} (-1)^{m'} i^{l_1+1} h_{l_1}^+(kR_{ij}) Y_{l_1, m' - m}(\hat{R}_{i,j}).$$

Here h_l^+ are Hankel functions, $Y_{l,m}$ are the spherical harmonics and $\vec{R}_{i,j}$ the vector joining site j to site i .

$$(45) \quad G_{i,j}^{L,L'} \neq 0 \text{ only if } i \neq j$$

Describe the site to site wave propagation.

$$\underline{h}_l^+(kr) \sim \frac{e^{ikr}}{kr} \text{ asymptotic behaviour for } kr \gg l$$

Phys. Rev. B 52, 15122 (1995) – see refs. therein

Chemistry – structure decoupling

The two important matrices appearing in the cross-section are related to the chemistry (T using only atom indexing):

$$(46) \quad T = \begin{pmatrix} t_0 & 0 & 0 & \dots & 0 \\ 0 & t_1 & 0 & \dots & 0 \\ \dots & \dots & \dots & \dots & \dots \\ 0 & 0 & \dots & t_{N-1} & 0 \\ 0 & 0 & \dots & 0 & t_N \end{pmatrix}$$

and to the geometry (G):

$$(47) \quad G = \begin{pmatrix} 0 & G_{0,1} & G_{0,2} & \dots & G_{0,N} \\ G_{1,0} & 0 & G_{2,0} & \dots & G_{1,N} \\ \dots & \dots & \dots & \dots & \dots \\ G_{N-1,0} & G_{N-1,1} & \dots & 0 & G_{N-1,N} \\ G_{N,0} & G_{N,1} & \dots & G_{N,N-1} & 0 \end{pmatrix}$$

Phys. Rev. B 52, 15122 (1995)

Electron interaction and structure are decoupled! In this approach the model optical potential is included in the scattering matrices t_i (irrespective of their positions). Conversely, the matrices G_{ij} contain only information on the geometrical dispositions of atoms i and j irrespective of their actual scattering power.

Multiple-scattering expansion

- Non-linear relationship between geometry and XAS signal:

$$\sigma \sim (I - GT)^{-1}$$

Non linearity: mathematical consequence of the strong coupling of the photoelectron with the surrounding atoms (more difficulties in analyzing XAS data).

- First approach: multiple scattering (MS) expansion. Where the norm of the GT matrix (maximum modulus of its eigenvalues) satisfies $\|GT\| < 1$ then the formal matrix expansion $T(I - GT)^{-1} = T(I + GT + GTGT + GTGTGT + \dots)$ is convergent and gives rise to the MS series.

The above condition will certainly hold above a given energy since not only the elements of the G matrix decrease like $1/\sqrt{E}$ but also $\|T\| = \max |t_i|$ tends to zero much more rapidly with energy. The convergence threshold is system dependent, typical values range from below the edge to a few Ry.

- Writing down the series we obtain:

$$(48) \quad \sigma(\omega) = \sigma_0 \left[1 + \sum_{i \neq 0} \chi_2^{0i0} + \sum_{\substack{i \neq j \\ i \neq 0, j \neq 0}} \chi_3^{0ij0} + \sum_{\substack{i \neq j \neq k \\ i \neq 0, k \neq 0}} \chi_4^{0ijk0} + \dots \right]$$

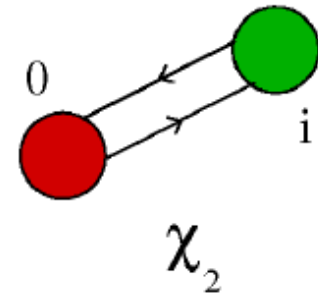
Multiple-scattering signals

The generic χ_n structural term is:

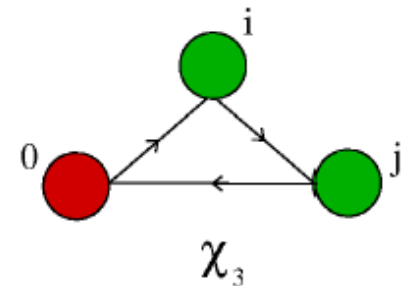
$$(49) \quad \chi_n^{0i\dots j0} = \mathfrak{S} \left(\frac{t_0^{l_0}}{\mathfrak{S}(t_0^{l_0})} \frac{1}{2l_0 + 1} \sum_{m_0} (\Xi^{0i\dots j0})_{L_0, L_0} \right)$$

and specifically $\Xi^{0i0} = G_{0,i}t_i G_{i,0}t_0$ for χ_2^{0i0} , $\Xi^{0ij0} = G_{0,j}t_j G_{j,i}t_i G_{i,0}t_0$ for χ_3^{0ij0} , and $\Xi^{0ijk0} = G_{0,k}t_k G_{k,j}t_j G_{j,i}t_i G_{i,0}t_0$ for χ_4^{0ijk0} . In this notation it is understood that the internal angular momentum indices have been saturated.

$$(50) \quad \chi_2^{0i0} = \mathfrak{S} \left(\frac{t_0^{l_0}}{\sin^2(\delta_0^{l_0})} \frac{1}{2l_0 + 1} \sum_{m_0} (G_{0,i}t_i G_{i,0}t_0)_{L_0, L_0} \right)$$



$$(51) \quad \chi_3^{0ij0} = \mathfrak{S} \left(\frac{t_0^{l_0}}{\sin^2(\delta_0^{l_0})} \frac{1}{2l_0 + 1} \sum_{m_0} (G_{0,j}t_j G_{j,i}t_i G_{i,0}t_0)_{L_0, L_0} \right)$$



Single-scattering approximation

- High energy limit: $kr_{ij} \gg 1$ (single-scattering approximation)

$$(53) \quad \sigma(\omega) \sim \sigma_0 \left[1 + \sum_{i \neq 0} \chi_2^{0i0} \right]$$

- Starting point for explicit calculation (given excitation channel l_0):

$$(54) \quad \chi_2^{0j0} = \Im \left(\frac{1}{\sin^2(\delta_0^{l_0})} \frac{1}{2l_0 + 1} \sum_{m_0} [t_0 G_{0,j} t_j G_{j,0} t_0]_{L_0, L_0} \right)$$

Using the relationship between phase-shift δ_j^l and the scattering matrix $t_i^l = \exp(i\delta_j^l) \sin(\delta_j^l)$ for the photoabsorbing atom, it becomes:

$$(55) \quad \chi_2^{0j0} = \Im \left(\frac{1}{2l_0 + 1} e^{2i\delta_0^{l_0}} \sum_{m_0} [G_{0,j} t_j G_{j,0}]_{L_0, L_0} \right).$$

High-energy limit

The explicit form of the reduced Hankel functions appearing in the propagator G is:

$$(56) \quad \underline{h}_l^+(kr) = i^{l+1} h_l^+(kr) = \frac{e^{ikr}}{kr} \sum_{t=0}^l \frac{(l+t)!}{(l-t)! t!} \left(\frac{i}{2kr}\right)^t$$

whose asymptotic behaviour for $kr \gg l$ is

$$(57) \quad \underline{h}_l^+(kr) \sim \frac{e^{ikr}}{kr}.$$

We then obtain the following expression for the single-scattering term:

$$(58) \quad \chi_2^{0j0} = \frac{(4\pi)^2}{2l_0 + 1} \Im \left[e^{2i\delta_0^{l_0}} \sum_{m_0} \sum_{l,m} \sum_{l',m'} C_{L_0,L'}^L \underline{h}_{l'}^+(kr_{0j}) Y_{l',m'}(\hat{r}_{0j}) \right. \\ \left. t_j^l \sum_{l'',m''} C_{L',L''}^{L_0} \underline{h}_{l''}^+(kr_{j0}) Y_{l'',m''}(\hat{r}_{j0}) \right]$$

$$(59) \quad C_{L,L''}^{L'} = \left[\frac{(2l+1)(2l'+1)(2l''+1)}{4\pi} \right]^{\frac{1}{2}} \begin{pmatrix} l & l' & l'' \\ 0 & 0 & 0 \end{pmatrix} \begin{pmatrix} l & l' & l'' \\ m & -m' & m'' \end{pmatrix} (-1)^{m'}$$

$C_{L,L''}^{L'}$ are the Gaunt coefficients expressed with the 3J symbols (see for example M. Rotenberg, the 3J and 6J symbols MIT press, Cambridge USA 1959).

MT single-scattering

Using the sum rules for Gaunt coefficients:

$$(60) \quad \sum_{m_0, m} C_{L_0, L'}^L C_{L, L''}^{L_0} = \left[\frac{(2l_0 + 1)(2l + 1)}{4\pi} \right] \begin{pmatrix} l_0 & l & l' \\ 0 & 0 & 0 \end{pmatrix}^2 (-1)^{m'} \delta_{l', l''} \delta_{m', m''}$$

$$(61) \quad \sum_{m'} (-1)^{m'} Y_{l', m'}(r \hat{o}_j) Y_{l', -m'}(r \hat{j}_0) = \frac{2l' + 1}{4\pi} (-1)^{l'}$$

we simplify the equation for χ_2 in this way

$$(62) \quad \chi_2^{0j0} = \Im \left(e^{2i\delta_0^{l_0}} \sum_l (2l + 1) t_j^l \sum_{l'} (2l' + 1) \begin{pmatrix} l_0 & l & l' \\ 0 & 0 & 0 \end{pmatrix}^2 \underline{h}_{l'}^{+2}(kr_0j) (-1)^{l'} \right).$$

This equation, exact within the muffin-tin approximation, can be further elaborated by exploiting the fact that the involved 3J symbol is different from zero only when the sum

$l_0 + l' + l''$ is even. In this case $(-1)^{(l_0+l+l')} = 1$ from which follows

$$(-1)^{(l_0+l)} = (-1)^{(l')} = (-1)^{(-l')} .$$

Plane-wave/small-atom approx.

Using the preceding equations χ_2 becomes:

$$(63) \quad \chi_2^{0j0} = (-1)^{l_0} \Im \left(e^{2i\delta_0^{l_0}} \sum_l (-1)^l (2l+1) t_j^l \sum_{l'} (2l'+1) \begin{pmatrix} l_0 & l & l' \\ 0 & 0 & 0 \end{pmatrix}^2 \underline{h}_{l'}^+(kr_{0j}) \right).$$

This “exact” equation for the single-scattering term can be then approximated by using the plane-wave, small-atom approximation for the spherical propagators $\underline{h}_l^+(kr) \sim \frac{e^{ikr}}{kr}$ and using the sum rule

$$(64) \quad \sum_{l'} (2l'+1) \begin{pmatrix} l_0 & l & l' \\ 0 & 0 & 0 \end{pmatrix}^2 = 1.$$

This leads to the following approximate equation for the single-scattering term:

$$(65) \quad \chi_2^{0j0} \sim (-1)^{l_0} \Im \left(e^{2i\delta_0^{l_0}} \sum_l (-1)^l (2l+1) t_j^l \frac{e^{2i(kr_{0j})}}{(kr_{0j})^2} \right).$$

The back-scattering amplitude for atom j can be written as:

$$(66) \quad f_j(\pi, k) = |f_j(\pi, k)| e^{i\phi_j(k)} = \frac{1}{k} \sum_l (2l+1) (-1)^l t_j^l$$

'EXAFS' formula

Using the preceding relationships we obtain:

$$(67) \quad \begin{aligned} \chi_2^{0j0} &\sim (-1)^{l_0} \Im \left(e^{2i\delta_0^{l_0}} |f_j(\pi, k)| e^{i\phi_j(k)} \frac{e^{2i(kr_{0j})}}{k(r_{0j})^2} \right) \\ &= (-1)^{l_0} \frac{|f_j(\pi, k)|}{k(r_{0j})^2} \sin \left(2kr_{0j} + 2\delta_0^{l_0}(k) + \phi_j(k) \right). \end{aligned}$$

The usual “EXAFS” formula for a particular dipole-selected channel l_0 can be recovered considering N_j neighboring atoms whose interatomic distances r_{0j} follow a Gaussian distribution of variance σ_j^2 :

$$(68) \quad \chi_2 \sim (-1)^{l_0} \sum_j \frac{|f_j(\pi, k)|}{k(r_{0j})^2} e^{-2k^2\sigma^2} e^{-2r_{0j}/\lambda(k)} \sin \left(2kr_{0j} + 2\delta_0^{l_0}(k) + \phi_j(k) \right).$$

where inelastic losses and finite core-hole lifetime are taken into account by a phenomenological term λ (“mean free path”).

This last equation is usually referred to as the “EXAFS” formula and can hold only for high photoelectron kinetic energies where the multiple-scattering series is usually rapidly convergent. Both single-scattering and plane-wave approximation have been shown to be a too crude approximation for the interpretation of the EXAFS signal.

MS signals vs structure

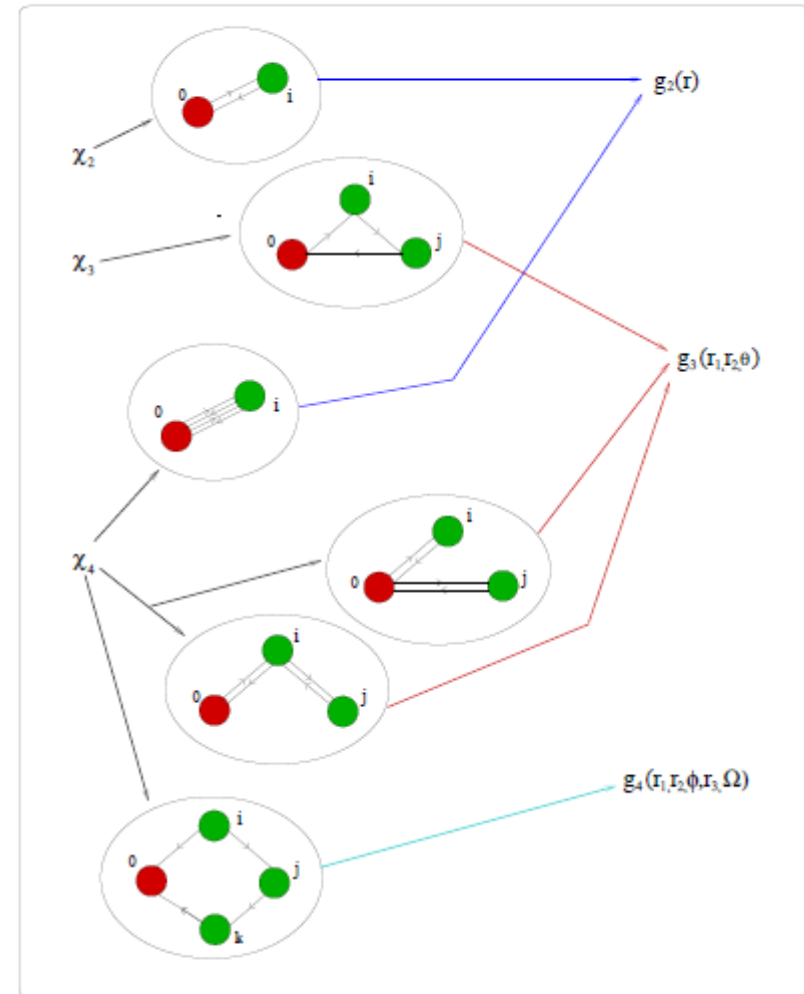
General features:

- The χ_n signals are oscillating functions of the type:

$$(52) \quad \chi_n(k) = A(k, R) \sin(kR_p + \phi(k, R))$$

where A and ϕ are smooth functions of k and of the geometrical parameters R . The relevant frequency of the signal is the path length R_p .

- The MS expansion has no simple relationship with the structure (geometry): χ_2 terms probe the relative position of atoms 0 and i , χ_3 terms probe the positions of the atoms 0, i and j . They are sensitive to the two-particle and three-particle distribution respectively. For χ_4 terms the situation becomes more complicated: a generic $0ijk0$ path probes four-particle correlations, but special paths like $0i0k0$ or $0ijj0$ and $0i0i0$ probe lower order correlations. In general at order n , in χ_n there are paths involving all particle distributions from 2 to n if n is even or from 3 to n if n is odd.



High energy limit: it is obtained when only the first χ_2 term is retained (single scattering approximation). The cross-section depends only on the two-particle distribution, but, even more important, the relation between structure and signal can be expressed as a linear functional of the radial distribution function.

The n-body expansion

• A different approach to the solution of the XAS structural problem is based on a n -body decomposition of the cross-section, which partially avoids the drawbacks related to the MS expansion. The main idea is to reduce the dimension of the problem to the actual local physical quantities of interest, related to n -atom properties where $n \ll N$ (N being the number of atoms of the system).

• Let us indicate, as usual, the photoabsorber with "0" and the surrounding atoms with $i, j, k \dots$. We define as the n -atom cross-sections for increasing n the quantities:

$\sigma(0) = \sigma_0$: atomic cross-section;

$\sigma(0, i)$ cross-section of the structure including atoms 0 and i only;

$\sigma(0, i, j)$ cross-section of the structure including atoms 0, i and j ;

$\sigma(0, i, j, k)$ cross-section of the structure including atoms 0, i, j and k .

• In the MT approximation these cross-sections can be easily calculated using the appropriate number of blocks in the G and T matrices.

• The irreducible n -body cross-sections $\sigma^{(n)}(0, i_1, \dots, i_{n-1})$ can be defined inductively starting from these quantities.

• For $n = 2$ it is the contribution due to the presence of a second atom i that is given by:

$$(1) \quad \sigma^{(2)}(0, i) = \sigma(0, i) - \sigma^{(1)}(0) = \sigma(0, i) - \sigma_0.$$

This is the irreducible two-body cross-section

n-body XAS cross-sections

- For $n = 3$ the cross-section for atoms 0, i and j can be decomposed into: the photoabsorber contribution, the two 0- i and 0- j two-body contributions, and an irreducible three-body contribution, that is given, by this definition as:

$$(2) \quad \sigma^{(3)}(0, i, j) = \sigma(0, i, j) - \sigma^{(2)}(0, i) - \sigma^{(2)}(0, j) - \sigma^{(1)}(0).$$

- Similarly the 4-body contribution is given by:

$$(3) \quad \begin{aligned} \sigma^{(4)}(0, i, j, k) &= \sigma(0, i, j, k) - \sigma^{(3)}(0, i, j) - \sigma^{(3)}(0, i, k) - \sigma^{(3)}(0, j, k) - \\ &- \sigma^{(2)}(0, i) - \sigma^{(2)}(0, j) - \sigma^{(2)}(0, k) - \sigma^{(1)}(0). \end{aligned}$$

- By induction, we can define the irreducible n -body contributions as:

$$(4) \quad \begin{aligned} \sigma^{(n)}(0, i, j \dots n) &= \sigma(0, i, j \dots n) - \sum \sigma^{(n-1)}(0, S(n-2)) - \\ &- \sum \sigma^{(n-2)}(0, S(n-3)) - \dots - \sum_i \sigma^{(2)}(0, i) - \sigma^{(1)}(0) \end{aligned}$$

Original refs.: Phys. Rev. B 52, 15122 and 15135 (1995)

where $S(m)$ indicates a choice of m elements among $1, 2 \dots N - 1$ and the sums are extended to all possible choices.

The XAS n-body expansion (GnXAS)

- On the other hand, the total cross-section for n atoms $\sigma(0, i, j \dots n)$ can be expanded in terms of the irreducible n -body cross sections of lower order. A useful expansion is thus obtained:

$$(5) \quad \sigma(0, i, j \dots, n) = \sigma_0 + \sum_i \sigma^{(2)}(0, i) + \sum_{(i,j)} \sigma^{(3)}(0, i, j) + \\ + \sum_{(i,j,k)} \sigma^{(4)}(0, i, j, k) + \dots + \sigma^{(n)}(0, i, j, \dots, n).$$

- The dimensionless quantities $\gamma^{(n)} = \sigma^{(n)} / \sigma_0$, represent the irreducible n -body contributions to the structural XAS term $\chi(\omega) = \frac{\sigma(\omega) - \sigma_0}{\sigma_0}$ and we arrive to an equivalent expansion for the dimensionless experimental structural signal χ that differs substantially from the MS series:

$$(6) \quad \chi(0, i, j \dots, n) = \sum_i \gamma^{(2)}(0, i) + \sum_{(i,j)} \gamma^{(3)}(0, i, j) + \\ + \sum_{(i,j,k)} \gamma^{(4)}(0, i, j, k) + \dots + \gamma^{(n)}(0, i, j, \dots, n).$$

Original refs.: Phys. Rev. B 52, 15122 and 15135 (1995)

Convergence

To discuss the convergence of the expansion in $\gamma^{(n)}$ signals, let us consider the two series expansions of the structural oscillation $\chi(k)$:

$$(13) \quad \chi(k) = \sum \chi_2 + \sum \chi_3 + \sum \chi_4 + \dots + \text{Res}_\chi^{(n)}$$

$$(14) \quad \chi(k) = \sum \gamma^{(2)} + \sum \gamma^{(3)} + \sum \gamma^{(4)} + \dots + \text{Res}_\gamma^{(n)}.$$

Assuming that the MS series is absolutely convergent, then the remainder $\text{Res}_\chi^{(n)}$ will satisfy the following inequality:

$$(15) \quad \text{Res}_\chi^{(n)} = \sum_{i>n} \chi_i \leq \sum_{i>n} |\chi_i| < \infty.$$

The remainder of the γ series, for any given order, will contain a smaller number of χ terms with respect to the remainder of the MS series, because many MS terms to any order are enclosed in the γ . As a consequence

$$(16) \quad \text{Res}_\gamma^{(n)} = \sum_{i>n} \gamma^{(i)} \leq \sum_{i>n} |\gamma^{(i)}| \leq \sum_{i>n} |\chi_i| < \infty,$$

and therefore also the series in the γ signals will be absolutely convergent.

• In general the rate of convergence of the series in the γ signals is better (not worse) than the rate of the χ series.

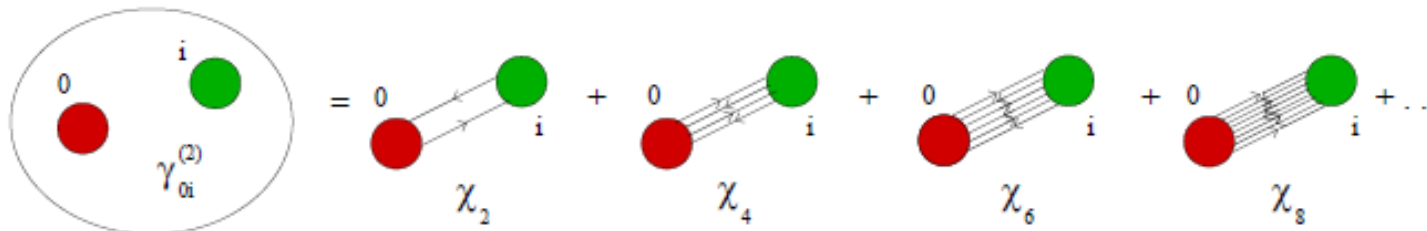
Irreducible n-body XAS signals

The irreducible n -body $\gamma^{(n)}$ signals are the central quantities in our approach, since they are associated with well precise n -body arrangements of the atoms.

- A simple linear relationship between structure (expressed in terms of 2, 3, 4, ... n -body distributions) and signal is obtained. The relationship contains a finite number of terms if the system is finite (cluster).
- Due to mean free path effects, the higher order n -body terms are generally smaller than the lower order ones, so that convergence with few terms is expected.
- Low-order $\gamma^{(n)}$ signals can be easily calculated with different methods (within GNXAS).

The corresponding MS expansion, pictorially depicted below, results:

$$(10) \quad \gamma^{(2)}(0, i) = \chi_2^{0i0} + \chi_4^{0i0i0} + \chi_6^{0i0i0i0} + \chi_8^{0i0i0i0i0} + \dots$$



Three-body signals

The MS series for $\gamma^{(3)}(0, i, j)$ can similarly be derived:

$$(11) \quad \gamma^{(3)} = \Im \frac{1}{\Im(t_0^{l_0})} \left[\frac{1}{3} \sum_{m_0} \right] \left\{ \begin{array}{l} \left(\begin{array}{ccc} t_0 & 0 & 0 \\ 0 & t_i & 0 \\ 0 & 0 & t_j \end{array} \right) \\ \sum_{n=1}^{\infty} \left[\left(\begin{array}{ccc} 0 & G_{0i} & G_{0j} \\ G_{i0} & 0 & G_{ij} \\ G_{j0} & G_{ji} & 0 \end{array} \right) \left(\begin{array}{ccc} t_0 & 0 & 0 \\ 0 & t_i & 0 \\ 0 & 0 & t_j \end{array} \right) \right]^n \end{array} \right\}_{L_0, L_0}^{0,0} - \gamma_{0i}^{(2)} - \gamma_{0j}^{(2)}.$$

By performing the matrix product, terms of any order in the scattering containing all three atoms 0, i and j , or simply 0 and i or 0 and j are obtained. These last two contributions are however compensated exactly by the terms arising from the $\gamma^{(2)}$ signals appearing with negative sign. As a consequence $\gamma_{0,i,j}^{(3)}$ equals the sum of all possible MS signals involving “all and only” 0, i e j in any possible sequence. The lowest order terms are the χ_3 signals corresponding to the sequences 0- i - j -0 and 0- j - i -0. Because of time reversal symmetry the two signals coincide and only one of them can be considered with double degeneracy. This obviously occurs for all the paths that, when reversed, generate a different sequence. The sequences that are symmetric under inversion occur instead only once and have a single degeneracy.

Irreducible n-body XAS signals

Finally, applying the previous rules to the $\gamma^{(4)}$ signal, which depends on the position of the atoms 0, i, j, k, we obtain:

$$(12) \quad \gamma^{(4)} = 2 \left(\chi_4^{0ijk0} + \chi_4^{0ikj0} + \chi_4^{0kij0} + \chi_5^{0i0jk0} + \chi_5^{0i0kj0} + \chi_5^{0j0ik0} + \chi_5^{0j0ki0} + \right. \\ \left. + \chi_5^{0k0ij0} + \chi_5^{0k0ji0} + \chi_5^{0ijik0} + \chi_5^{0ikij0} + \chi_5^{0jijjk0} + \chi_5^{0jkji0} + \chi_5^{0kikj0} + \right. \\ \left. + \chi_5^{0kjkio} + \chi_5^{0ijki0} + \chi_5^{0jikj0} + \chi_5^{0kijk0} + \dots O(\chi_6) \dots \right).$$

this contribution is important in some cases (especially when atoms are in a linear configurations, “focusing” effect in three-body and four-body terms).

The expressions becomes rapidly more cumbersome as the body order n is increased.

It is important to realize that while the MS expansions for the $\gamma^{(n)}$ have a meaning only in the case that the expansion relative to all the matrix inversions included in their definition converge (notice however that their convergence requirements are in general different from that relative to the matrix inversion of the whole cluster), the $\gamma^{(n)}$ signals always exist and can be calculated using the exact inversion.

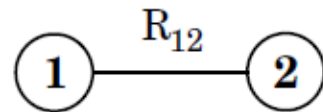
- The advantage of incorporating in a few $\gamma^{(n)}$ signals a large (infinite) number of MS terms is evident from a practical point of view. Moreover, this is also very useful from the physical point of view. Indeed different MS term are not independent if they involve scattering processes on the same sets of atoms.
- $\gamma^{(n)}$ signals are, like the χ_n , oscillating functions of the photoelectron wavevector modulus k . They show a broad frequency spectrum whose dominant frequency is that associated with the shortest path of the corresponding MS series.

n-body cluster analysis

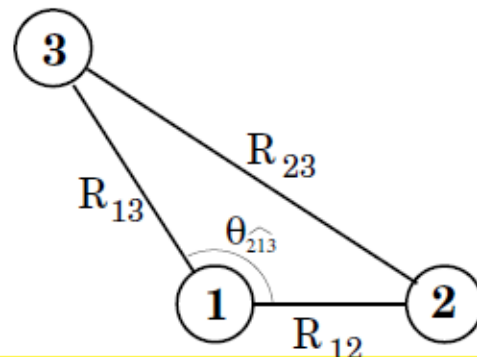
For calculating a XAS signal associated with a given cluster it is necessary to identify the relevant n -body configurations. Identification of configurations can be done assuming a single photoabsorbing site (single photoabsorber or multiple atoms placed in equal positions by rotation and translations), and can be generalized for multiple prototypical photoabsorbers.

The irreducible n -body configurations around a given atom 0, and their multiplicities, are identified by considering all the different arrangements involving couples of atoms $(0, i)$, triplets of atoms $(0, i, j)$, quadruplets of atoms $(0, i, j, k)$, This can be done by introducing a natural, rotationally invariant, set of distances and angles that is associated in some unambiguous way to the configuration.

- In the case of a two-body configuration the only rotationally invariant coordinate is simply the distance $R_{0,i}$.



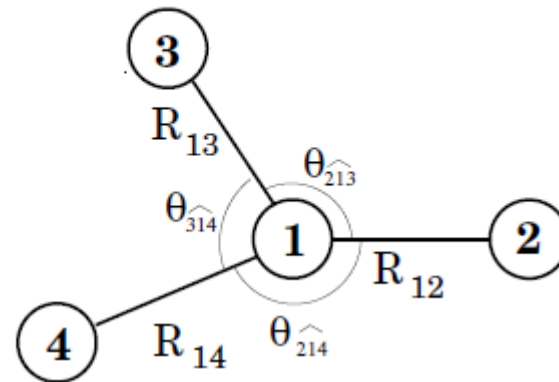
- In the case of a three-body configuration a convenient choice it is possible to use the two shortest distances among $R_{0,i}$, $R_{0,j}$, and $R_{i,j}$, and the angle in between. This choice is physically meaningful because the shortest bonds are in general real chemical bonds and the angle in between is a real bond-angle.



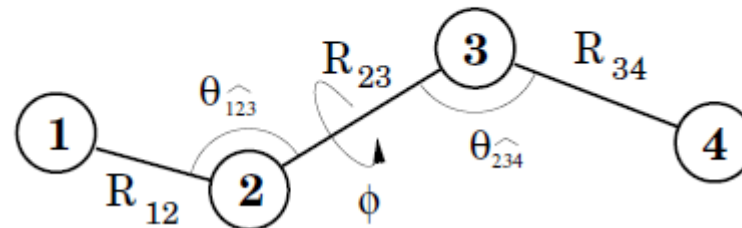
4-body topology

4-body configurations are more complicated, indeed if one wishes to specify the geometry using three distances and three angles there are already two choices: either the three bonds are joined end by end forming a “chain” or they are bound to the same center, forming a “star”. Criteria can be established, however, to make this choice unique. Again this variety reflects the different physical situations encountered when parameterizing say linear molecules or aggregates of atoms with a well defined center.

star 4-body conf.



chain 4-body conf.



Multiple photoabsorbers

In a periodic structure (like a simple crystal) there will be an infinite number of equivalent photoabsorbers, thus a given n -body arrangement may contain m atoms (with $1 \leq m \leq n$) of the photoabsorber atomic number.

This atomic configuration will give rise to m different $\gamma^{(n)}$ terms. In the $m > 1$ case the signals will be generally different (apart from permutational symmetry) although associated with the same geometrical structure. Moreover, they have a similar frequency and can be described by the same structural parameters.

As a consequence, in the spirit of reducing the independent components of $\chi^{(k)}$, we define the total γ signals γ_T as a the sum of all the related signals originating from the same structural arrangements of atoms i_1, \dots, i_n with the photoabsorber placed in any non-equivalent position:

$$(17) \quad \gamma_T^{(n)}(i_1, i_2, \dots, i_n) = \sum_j^{(i_j=0)} \gamma^{(n)}(i_j, \text{Perm}(i_k, (k \neq j)))$$

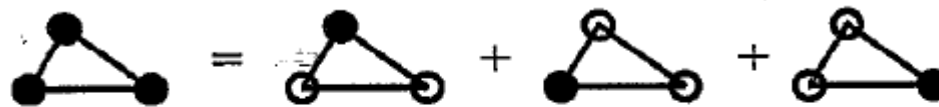


FIG. 3. Pictorial view of the definition of the total γ signal for a general triangular configuration of equivalent atoms.

n-body hierarchy

There is a hierarchical relationships between different n -body configurations: a n -body configuration contains several $n - m$ -body sub-configurations that are not independent. This allows to reduce the number of n -body coordinates just to the independent ones. For example, the inclusion of a distant coordination shell of atoms is associated with a new two-body signals, but will also generate higher order signals involving the atoms of the inner shells. Very often, it is physically meaningful to associate them in an effective shell signal, denoted by $\eta^{(n)}$:

$$(18) \quad \eta^{(n)} = \gamma^{(n)}(\dots) + \sum_{j=2}^{n-1} \gamma^{(j)}$$

A typical example is the second shell contribution which usually gives rise to detectable three-body signal. The three-body signal plus the two-body second shell signal will be in this case the $\eta^{(3)}$ signal associated with the second shell.



FIG. 4. Pictorial view of the definition of the $\eta^{(3)}$ signal associated with a typical distant (second) shell contribution.

Ordering and selection of n-body signals

- Frequency. Each n -body structure is defined by a set of coordinates, by the types of the atoms in the various positions, by the position of the photoabsorber, and by a characteristic dominant frequency, that is the length of the shortest path involving all of the atoms in the configuration (roughly corresponding to the position of the Fourier Transform peak).
- Ordering. This characteristic frequency allows to arrange the various n -body configurations in their “natural order”. The most important configurations will be those associated with the lowest frequencies, that is, the two-body first neighbor configuration with a length of $2R_b$. The most important three-body configuration will be associated with a frequency not smaller than $3R_b$ (equilateral triangle). In many open systems the shortest three-body path is much longer.
- Selection. Any experimental signal will show a natural upper frequency cutoff R_c , limited by experimental resolution or signal intensity, which will select automatically only a finite number of n -body structures. In particular also the order of maximum number of bodies involved will be limited, by frequency and intensity. In the interpretation of the signal of a completely unknown structure it is possible to make an “a-priori” selection of the relevant n -body configurations thus limiting considerably the number of unknowns.

In light of this cluster analysis we see that the XAS signal is actually dependent only on a limited number of distribution functions (n body configurations) which can be easily identified and analysed.

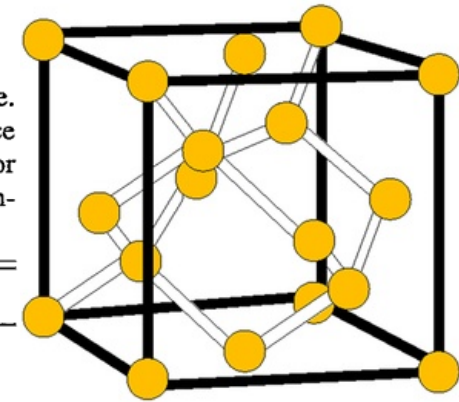
n-body structures for crystals

TABLE IV. Pair and triplet contributions in the diamond structure. The distances are reported in units of the nearest-neighbor distance R , the angles are in degrees. The degeneracy (Deg.) is specified for each configuration. The photoabsorber position for the triplet configurations is also specified (Pos.). Position 1 corresponds to the vertex between the two short bonds, position 2 is at the end of the first bond (with length R_1) and position 3 is at the end of the second bond.

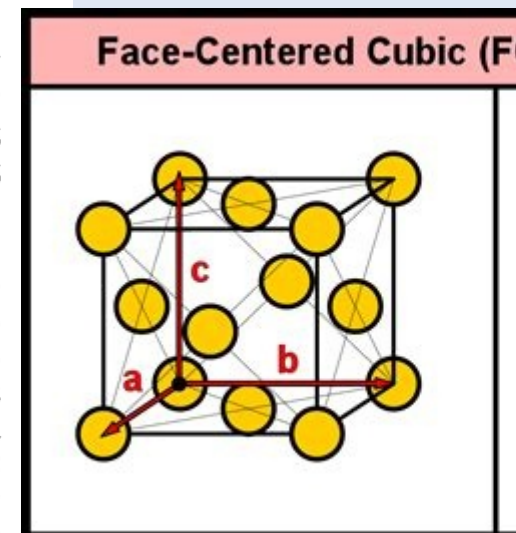
Peak	R_1/R	R_2/R	θ ($^\circ$)	Deg.	Pos.	$R_{\text{path}}/2R$
Pair distribution						
1	1			4		1
2	$\frac{2}{3}\sqrt{6}$			12		1.633
3	$\frac{1}{3}\sqrt{33}$			12		1.915
4	$\frac{4}{3}\sqrt{3}$			6		2.309
5	$\frac{1}{3}\sqrt{57}$			12		2.517
6	$2\sqrt{2}$			24		2.828
7	3			16		3
8	$\frac{4}{3}\sqrt{6}$			12		3.266
Triplet distribution						
1	1	1	109.47	6	1	1.816
				12	2	1.816
2	1	$\frac{2}{3}\sqrt{6}$	90.00	24	1	2.274
				24	2	2.274
				24	3	2.274
3	$\frac{2}{3}\sqrt{6}$	$\frac{2}{3}\sqrt{6}$	60.00	24	1	2.449
4	1	$\frac{2}{3}\sqrt{6}$	144.74	12	1	2.575
				12	2	2.575
				12	3	2.575

TABLE VI. Pair and triplet contributions in the fcc structure. The distances are reported in units of the nearest-neighbor distance R , the angles are in degrees. The degeneracy (Deg.) is specified for each configuration. The photoabsorber position for the triplet configurations is also specified (Pos.).

Peak	R_1/R	R_2/R	θ ($^\circ$)	Deg.	Pos.	$R_{\text{path}}/2R$
1	1			12		1
2	$\sqrt{2}$			6		$\sqrt{2}$
3	$\sqrt{3}$			24		$\sqrt{3}$
4	2			12		2
5	$\sqrt{5}$			24		$\sqrt{5}$
6	$\sqrt{6}$			8		$\sqrt{6}$
1	1	1	60	24	1	1.5
2	1	1	90	12	1	1.707
				24	2	1.707
3	1	1	120	24	1	1.866
				48	2	1.866
4	1	1	180	6	1	2
				12	2	2
5	1	$\sqrt{2}$	90	24	1	2.073
				24	2	2.073
				24	3	2.073
6	1	$\sqrt{3}$	73.22	48	1	2.232
				24	3	2.232
7	1	$\sqrt{2}$	135.00	24	1	2.325
				24	2	2.325
				24	3	2.325



(a) Si



XAS relationship with atom distribution

Having defined the irreducible $\gamma^{(n)}$ MS signals, the general expression of the XAS structural term is given in terms of the n -body distribution functions $g_n(r)$ (r is a generic set of n -body coordinates):

$$\begin{aligned}
 \langle \chi(k) \rangle = & \int_0^\infty dr 4\pi r^2 \rho g_2(r) \gamma^{(2)}(r, k) + \int dr_1 dr_2 d\phi 8\pi^2 r_1^2 r_2^2 \sin(\phi) \rho^2 g_3(r_1, r_2, \phi) \\
 & \times \gamma^{(3)}(r_1, r_2, \phi, k) + \int dr_1 dr_2 d\phi dr_3 d\Omega 8\pi^2 r_1^2 r_2^2 r_3^2 \sin(\phi) \rho^3 g_4(r_1, r_2, \phi, r_3, \Omega) \\
 (19) \qquad & \qquad \qquad \qquad \qquad \qquad \qquad \qquad \qquad \qquad \qquad \times \gamma^{(4)}(r_1, r_2, \phi, r_3, \Omega, k) \cdots \cdots
 \end{aligned}$$

The integrals, because of the short range nature of the Kernels $\gamma^{(n)}$, are actually limited to a region of linear dimensions of the order of few Å. This is due to the strong electron interaction (mean free path).

This equation should be compared with the well known expression for the static structure factor (disordered system) which can be measured by using x-ray or neutron diffraction:

$$(20) \qquad S(k) = 1 + \frac{4\pi\rho}{k} \int_0^\infty (g_2(r) - 1) r \sin(kr) dr.$$

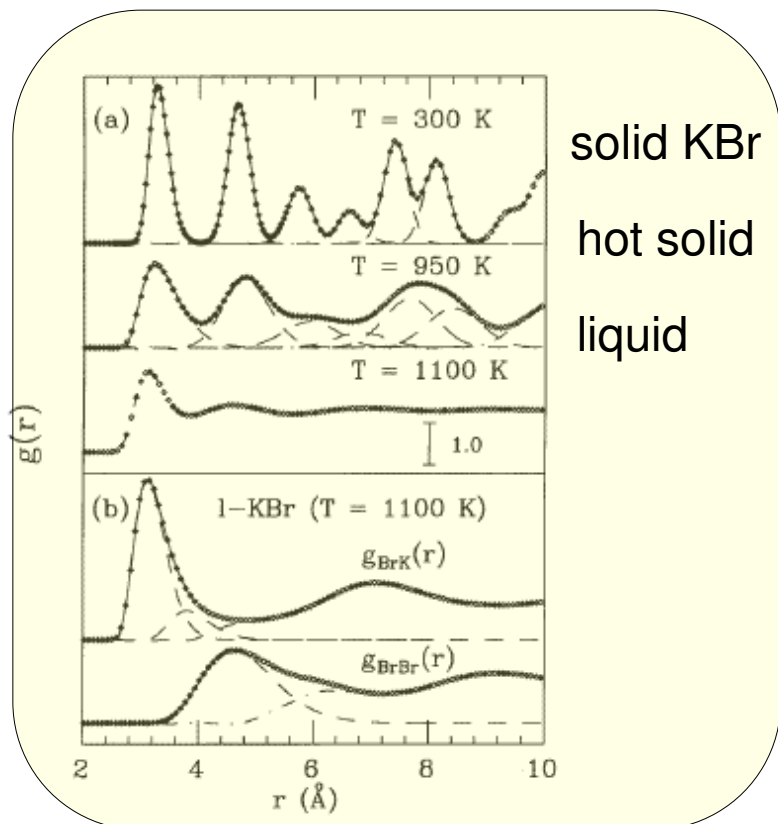
The different nature of the Kernels, however, makes the structural information on the $g_2(r)$ obtainable in the two cases largely complementary (short vs. medium range information). Moreover, XAS can give information beyond the pair distribution!

For crystals, where diffraction gives obviously a richer information about atomic positions, XAS provides unique data about local correlated vibrations.

Peak-fitting of the pair distribution

Structural refinement of the raw data through MS calculation of the XAS cross section (GNXAS $\rightarrow \gamma^{(n)}$ signals, corresponding to $g^{(n)}$ distributions)

- the distance distribution is assumed to be a superposition of distinct peaks (“shells”) whose parameters (N, R, σ^2, \dots) are fitted to the experimental data
- valid also for reconstructing the $g(r)$ in simple [1] and binary [2] liquids introducing physical constraints accounting for the density and the compressibility of the system



Needs:

- Extension of the refinement scheme to multi-component systems and higher-order distributions
- Model independent approach
- Simultaneous refinement of short and long-range order (XAS+diffraction)

[1] A. Filipponi, Journal of Physics: CM 13, R23 (2001)

[2] Angela Trapananti and Andrea Di Cicco

Phys. Rev. B 70, 014101 (2004)

<http://gnxas.unicam.it>

Configurational average

- *The effect of configurational disorder or thermal vibrations can be easily calculated in the case of small disorder, that is in the presence of a well defined (isolated) peak, not necessarily Gaussian, in the distribution function. This includes the thermal broadening of molecular or crystalline peaks. It can be used to treat the case of moderate structural disorder in glassy covalent systems but where the peaks are not any more well defined (liquids) different average methods should be used.*
- *MS signals $\chi_n(k)$, n -body signals $\gamma^{(n)}(k)$ or effective shell signals $\eta^{(n)}(k)$ can be treated in the same way. In all of these cases the signal, indicated generically by $\chi(k)$, can be written in terms of the amplitude $A(k, r)$ and phase $\psi(k, r)$ functions as*

$$(21) \quad \chi(k) = \Im A(k, r) \exp[i\psi(k, r)] = A(k, r) \sin[\psi(k, r)]$$

where r indicates a set of geometrical coordinates which are sufficient to describe correctly the signal.

$\psi(k, r) = kR_p + \phi(k, r)$ (R_p is the dominant frequency) and $A(k, r)$ are usually smooth functions of k, r .

- *$P(r)$ is the normalized probability density describing a peak of the appropriate n -body distribution function (configuration degeneracy, or CN for $n = 2$, being a trivial multiplicative factor). For $n = 2$,*

$$P(r) = 4\pi r^2 \rho g_2(r)$$

- *The configurational average of the signal over the peak distribution function $P(r)$ is given by:*

$$(22) \quad \langle \chi(k) \rangle = \Im \int dr A(k, r) \exp[i\psi(k, r)] P(r).$$

Moderate disorder

Small disorder: $P(r)$ has a maximum in position r_0 and decrease rapidly to 0 for strongly distorted geometries. Amplitude and phase of the γ signals can be calculated at the mean value r_m ($r_m = r_0$ for a Gaussian distribution) using a Taylor series:

$$(23) \quad A(k, r) = A_0(k, r)|_{r=0} + A_1(k, r)|_{r=0} \cdot r + \frac{1}{2} (r, A_2(k, r)|_{r=0} r) + O(r^3)$$

$$(24) \quad \psi(k, r) = \psi_0(k, r)|_{r=0} + \psi_1(k, r)|_{r=0} \cdot r + \frac{1}{2} (r, \psi_2(k, r)|_{r=0} r) + O(r^3)$$

where $A_j(k, r)|_{r=0}$ (briefly A_j in the following) are the j^{th} order derivatives with respect to all of the geometrical coordinates calculated for the mean r value. A similar notation has been used for the ψ functions, they are in general symmetric tensors of rank j (r origin translated to r_m).

Therefore, when such a low-order expansion is sufficient, we have:

$$(25) \quad \langle \chi(k) \rangle = \mathfrak{S} \int dr \left[A_0 + A_1 \cdot r + \frac{1}{2} (r, A_2 r) + O(r^3) \right] \exp \left(i \left[\psi_0 + \psi_1 \cdot r + \frac{1}{2} (r, \psi_2 r) + O(r^3) \right] \right) P(r).$$

Average of XAS signals

The average can be written isolating the lower order terms in amplitude and phase and writing the Taylor expansion for the amplitude as a differential operator with respect to ψ_1 , which is the conjugated variables of r :

$$(26) \quad \langle \chi(k) \rangle = \Im A_0 \exp(i\psi_0) \left[1 + \frac{1}{iA_0} A_1 \cdot \frac{\partial}{\partial \psi_1} - \frac{1}{2A_0} \left(\frac{\partial}{\partial \psi_1}, A_2 \frac{\partial}{\partial \psi_1} \right) + O\left(\frac{\partial^3}{\partial \psi_1^3}\right) \right] \int dr P(r) \exp(i\psi_1 \cdot r) \exp\left[\frac{i}{2}(r, \psi_2 r) + O(r^3)\right].$$

This is the most general expression for the damping of structural signals which occurs in the XAS case: the initial factors before the large square bracket represent the undamped signal, the rest is a complex corrective factor.

The amplitude expansion generates a differential operator, in square brackets, that acts on the last integral term.

- The integral, neglecting the last exponential term, i.e. neglecting ψ_2 and the successive terms in the phase expansion, is simply the characteristic function of the probability distribution $P(r)$. More specialized expressions can be derived, for specific $P(r)$ models and with the Taylor expansions truncated to some lower order.

- In the limit of a delta function shaped $P(r)$, the corrective factor tends to 1 irrespective of A_1 , A_2 , ψ_1 , and ψ_2 , and $\langle \chi(k) \rangle$ equals the undamped signal.

- Special cases occur when a particular geometrical parameter has an extremum for the equilibrium configuration. Then the corresponding first derivatives vanish and the first non-trivial term are the second order derivatives. An example is given by a 3-atom collinear configuration described by a 180° bond angle. Clearly the signal is affected in the same way by positive or negative angle displacements and therefore the Taylor expansion must be even in the angular coordinate.

Gaussian n-body distributions

A Gaussian n dimensional distribution can be written as:

$$(27) \quad P^{(n)}(r)dr = \frac{1}{(2\pi)^{n/2}} \frac{1}{\det(M^{1/2})} \times \exp \left[\frac{-(r, M^{-1}, r)}{2} \right] dr$$

When $n = 1$ we have a simple radial distribution and $M = \sigma^2$. For a generic triplet distribution the covariance matrix depends on six independent parameters

$$(28) \quad M = \begin{pmatrix} \sigma_1^2 & \sigma_{1,2}^2 & \sigma_{1,\theta}^2 \\ \sigma_{1,2}^2 & \sigma_2^2 & \sigma_{2,\theta}^2 \\ \sigma_{1,\theta}^2 & \sigma_{2,\theta}^2 & \sigma_\theta^2 \end{pmatrix}$$

where the suffix 1, 2, and θ indicate first, second bond and angle respectively.

The diagonal parameters are the variances of the coordinates, while the off-diagonal terms express the correlation between bond-bond or bond-angle vibrations. Since the matrix must be positive defined, it is useful to define the dimensionless correlation parameters as $\rho_{ij} = \sigma_{ij}^2 / \sqrt{\sigma_i^2 \sigma_j^2}$ that satisfy $-1 \leq \rho \leq 1$. In cases of particular symmetries the number of independent parameters is reduced. For an isosceles triangle where bonds 1 and 2 are equivalent $\sigma_1^2 = \sigma_2^2$ and $\rho_{1,\theta} = \rho_{2,\theta}$ with four independent parameters. For an equilateral triangle parameterized with the length of the three equivalent bonds as coordinates there are only two independent quantities: bond variance σ_1^2 and correlation $\rho_{1,1'}$.

Gaussian disorder – simple limits

A simple analytical expression is obtained for a Gaussian distribution of a generic n -body configuration:

$$(29) \langle \chi(k) \rangle = A_0 \sqrt{1 + \left[\frac{(A_1, M, \psi_1)}{A_0} \right]} \times \exp \left(- \frac{(\psi_1, M, \psi_1)}{2} \right) \sin \left[\psi_0 + \frac{(A_1, M, \psi_1)}{A_0} \right]$$

and similar expressions can be obtained for non-gaussian distributions (example of the Γ function).

- For a simple χ_2 term the usual EXAFS “Debye-Waller” like factor is recovered neglecting the r dependence in ϕ and A_1 :

$$\begin{aligned} \psi_0(k, r) &\sim 2kR + \phi(k, r) \\ \psi_1(k, r) &\sim 2k \\ (\psi_1, M, \psi_1) &\sim 4k^2 \sigma^2 \\ (A_1, M, \psi_1) &\sim 0 \end{aligned}$$

(30)

$$(31) \quad \langle \chi_2(k) \rangle = A_0 \exp \left(- (2k^2 \sigma^2) \right) \sin [2kR + \phi(k, r)]$$

XAS structural refinement strategy

- The non-linear minimization is performed using the raw absorption data $\alpha(E_i)$ including noise (not the $\chi(k)$ or filtered data). The model absorption spectrum $\alpha_m(E_i)$ thus include background modelling:

$$(32) \quad \alpha_m(E_i) = \alpha_{bkg}(E_i) + \alpha_{exc}(E_i) + [1 + \chi_m(E_i)] \alpha_0(E_i)$$

where

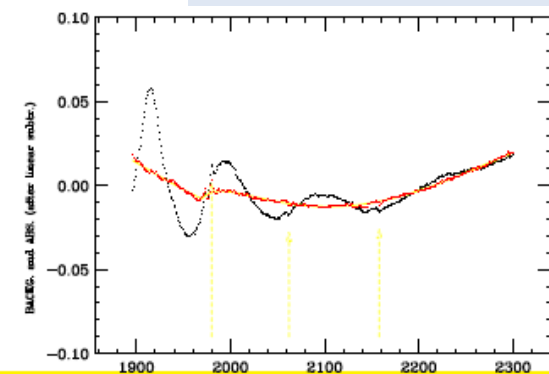
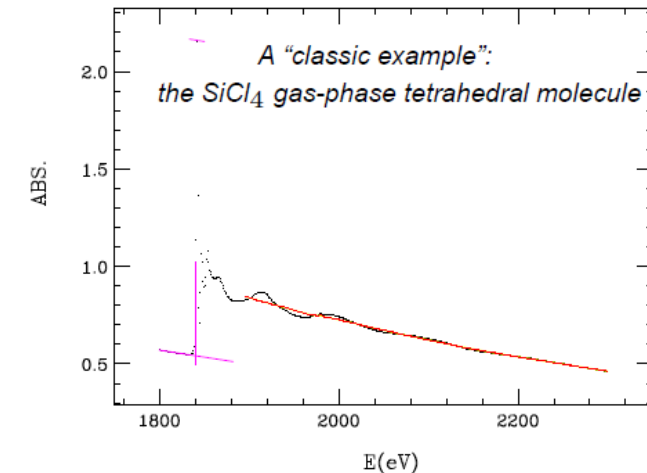
$\alpha_0(E_i) = J\sigma_0(E_i)$ is the atomic absorption coefficient

$\alpha_{bkg}(E_i)$ is a smooth polynomial background

$\alpha_{exc}(E_i)$ accounts for multi-electron excitation channels

- Simultaneous modelling of background and signal ($\chi_m(E_i)$) significantly reduces the introduction of systematic errors in the interpretation of the structural signal. Same approach for multi-edge studies:

$$(33) \quad \alpha_m(E_i) = \alpha_{bkg}(E_i) + \alpha_{exc}(E_i) + \sum_{j=1}^{NXAS} [1 + \chi_m^j(E_i)] \alpha_0^j(E_i)$$

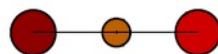
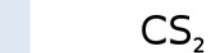
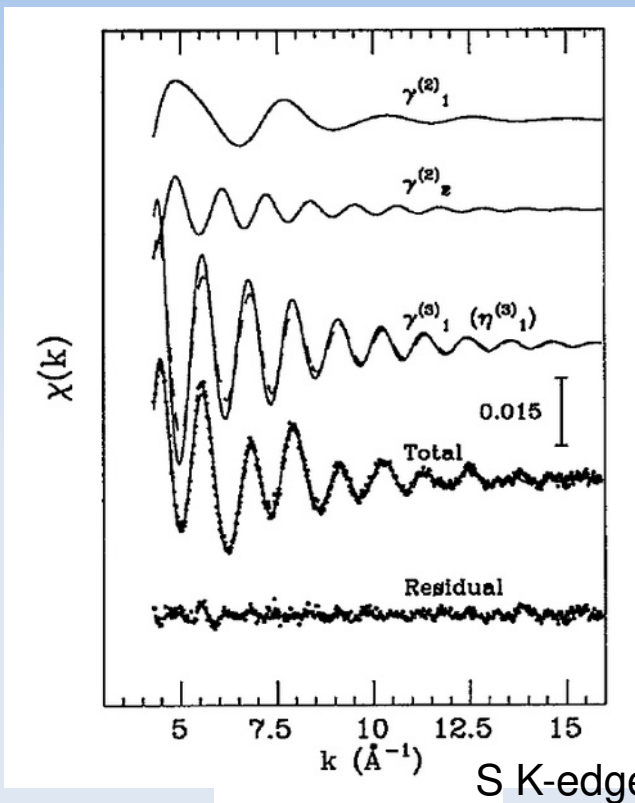


Phys. Rev. B 53, 6174 (1996), Phys. Rev. B, 62, 12001 (2000)

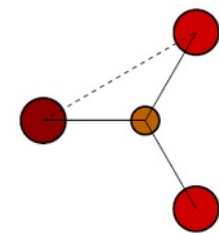
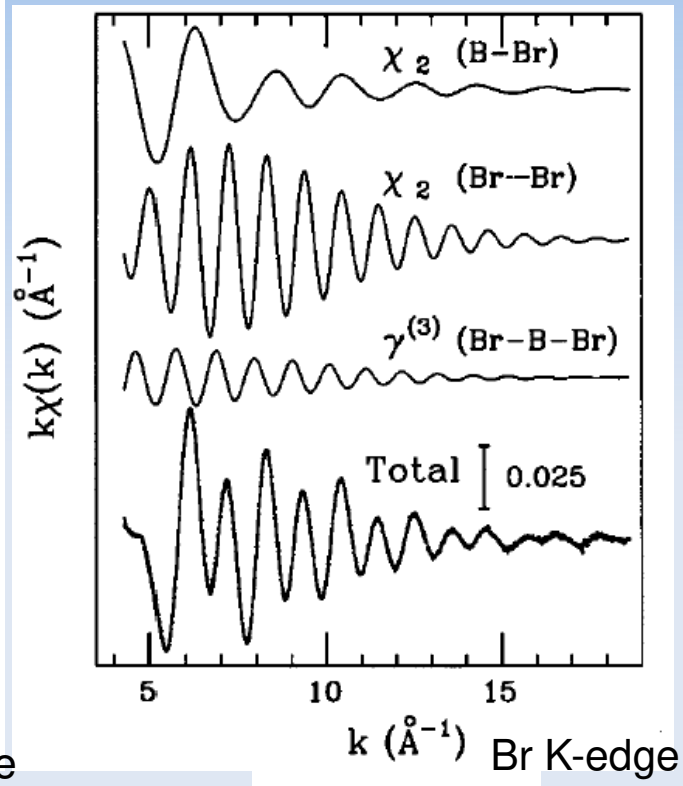
J. Phys. B, At. Mol. and Opt. Phys. 25, 2309 (1992)

Accuracy of XAS structure refinements: molecules

- Single and multiple-edge XAS refinements of gas-phase systems (using MS simulations and peak-fitting) have been shown to provide an accurate tool for measuring the distance (and angle) distributions
- Results have been found to be *in agreement* with electron diffraction data
- *Accuracy* in average distance determination can easily reach 0.002 Ang.
- *New information* on bond and angle distributions can be obtained



Phys. Rev. B 52, 15122 (1995)



Journal of Chemical Physics 109, 5356 (1998)

Accuracy of XAS structure refinements: crystals

XAS refinements of simple crystalline systems (using MS simulations and peak-fitting) can probe the short-range distribution accurately

- Structural results can enrich the information obtained by XRD/ND.
 - Access to correlated vibrations (related to the phonon density of states)
- XAS provides direct and unique information about the deviation from the harmonic approximation (gaussian distribution of distances)

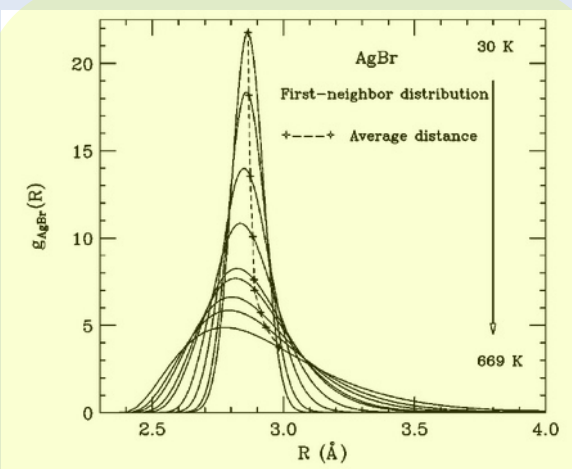
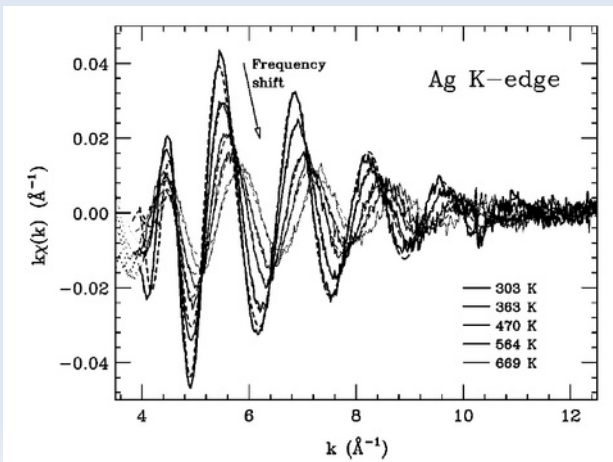
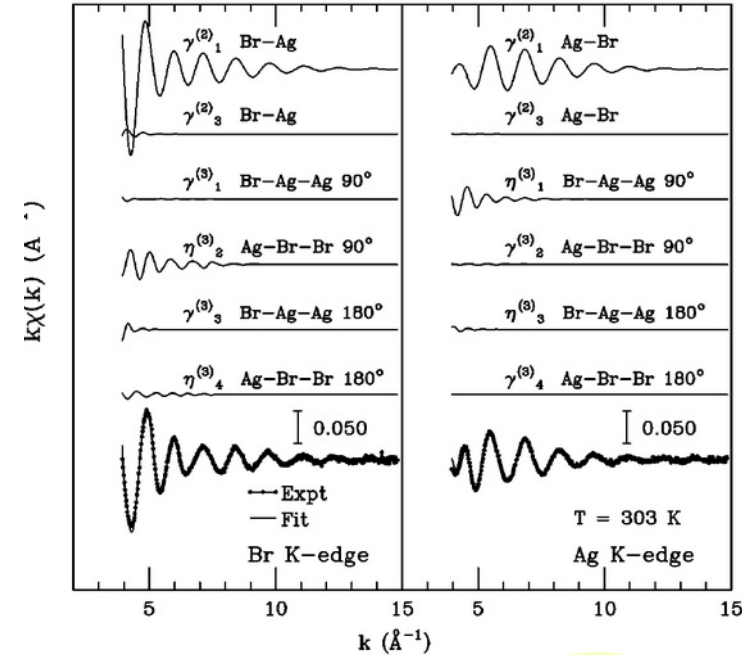
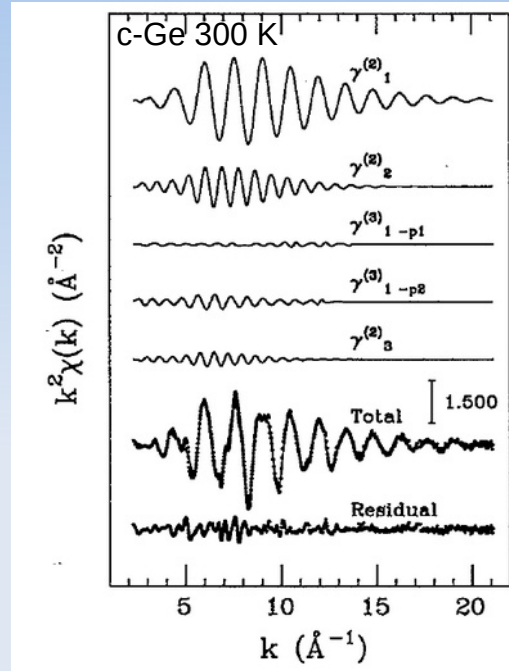
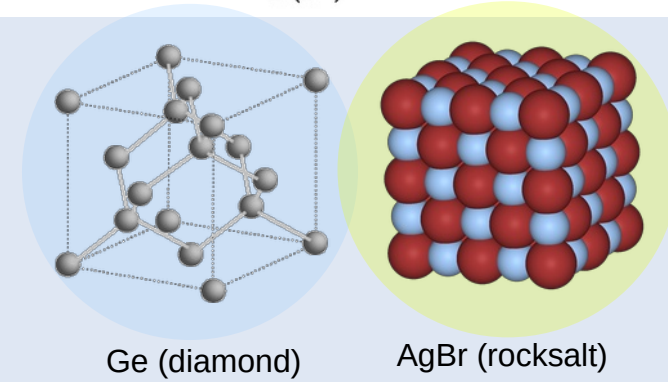


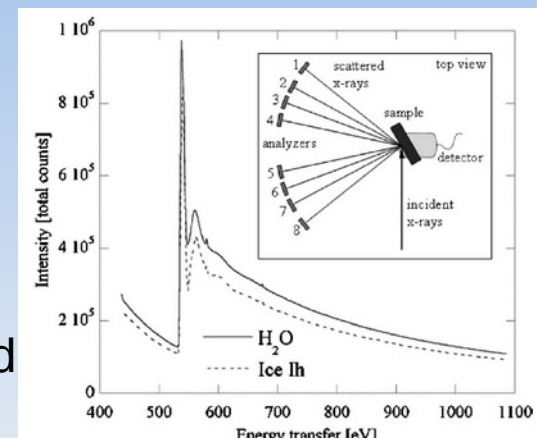
FIG. 10. First-neighbor AgBr distribution as a function of temperature. The average distance increases as a result of the thermal expansion, while the most probable value and the foot of the distribution shift toward shorter distances.



Phys. Rev. B, 62, 12001 (2000)

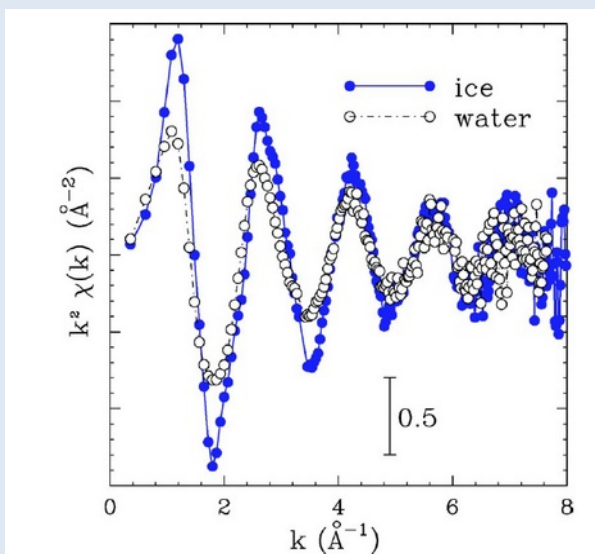
A look on “new” developments ...

- XAFS measured by x-ray Raman scattering
- bulk-sensitive XAFS of light elements (like oxygen in water)
- This photon-in photon-out technique (low counting rate) is now readily available (third generation synchrotrons) a
- High-quality XAFS at the O K-edge (543 eV) in water and ice measured at APS (Argonne) at the ID18 undulator beamline (6.9-7.5 keV)

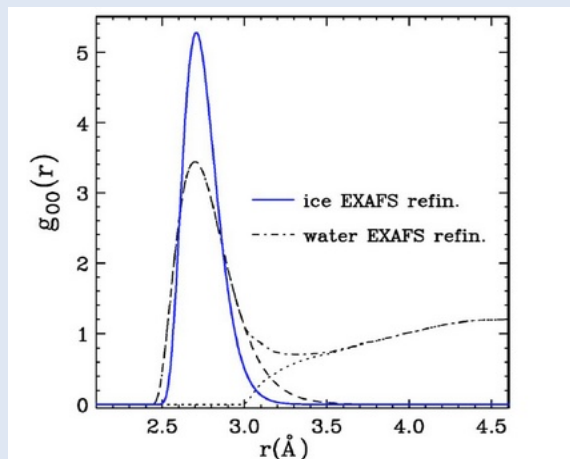


THE JOURNAL OF CHEMICAL PHYSICS 127, 174504 (2007)

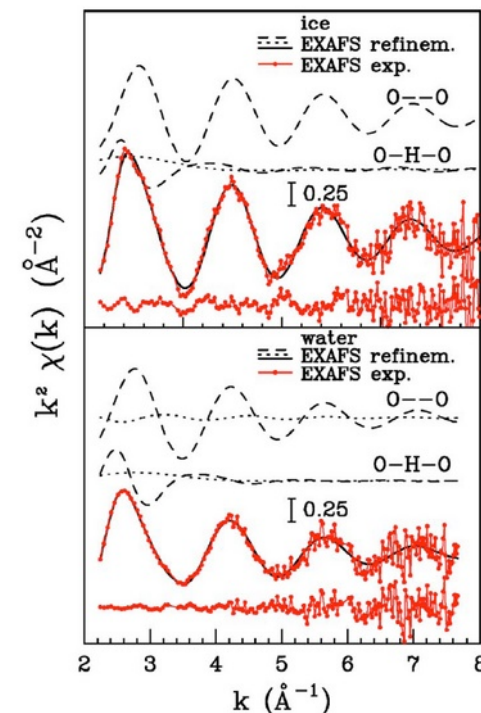
Nearest-neighbor oxygen distances in liquid water and ice observed by x-ray Raman based extended x-ray absorption fine structure



G. 2. (Color online) Comparison of x-ray Raman based $k^2(k)$ EXAFS



4. (Color online) Reconstructed RDF for water and ice based on re-



3. (Color online) Refinement of EXAFS from ice and water incl

Ultrafast XAS at FELs

Ultrafast XAS measurements at FELs can pump/probe (disordered) matter under extreme/transient conditions

PHYSICAL REVIEW B 90, 220303(R) (2014)

Interplay of electron heating and saturable absorption in ultrafast extreme ultraviolet transmission of condensed matter

Several shot-by-shot experiments were performed using hard and soft x-ray at different facilities

Challenging experiments and new experimental and theoretical problems

Al (100 nm) thin film, for EUV radiation and fluence above 1 J/cm² visible deviations due to saturation and electron heating effects are measured

Struct. Dynamics, vol 3. 023604 (2016)

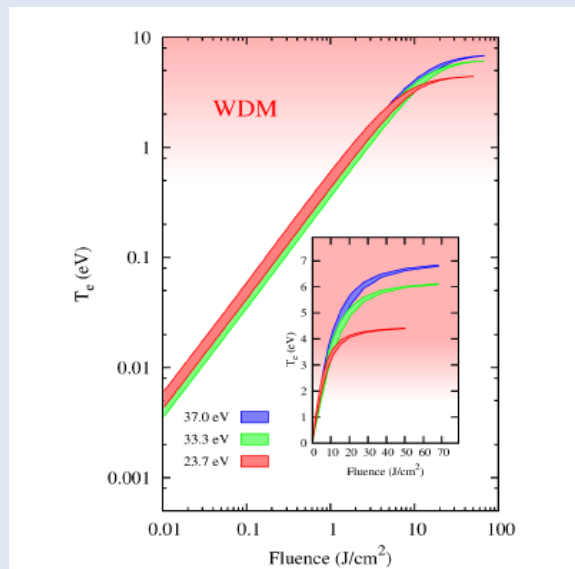
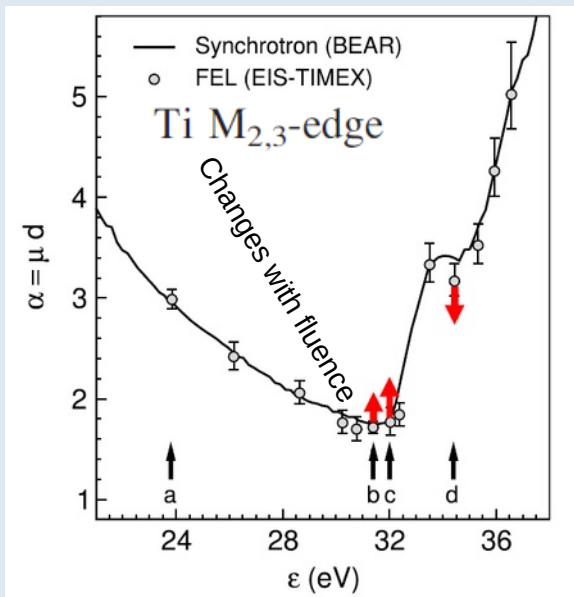


FIG. 4. Estimated electron temperature in the 100 nm thick Al thin film as a function of incoming fluence at different

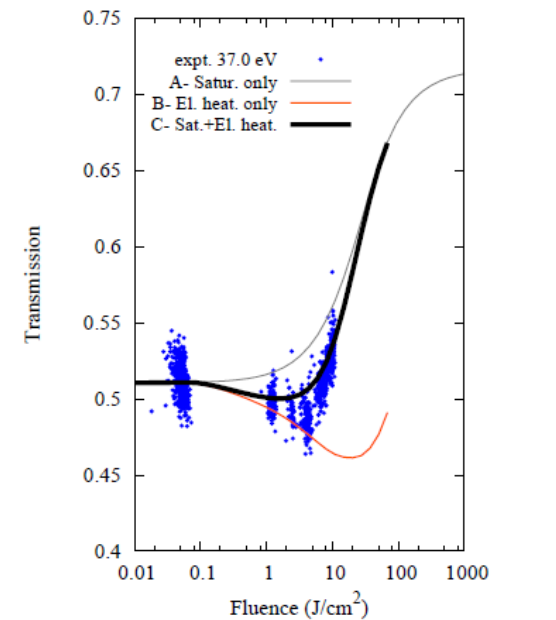


FIG. 3. Experimental EUV transmission data compared with different calculations (see text). Curve A includes only optical saturation phenomena without accounting for temperature effects; curve B includes electron heating but neglects saturation phenomena; curve C takes into account both electron heating and saturation effects.

Conclusions

XAS techniques available at SR facilities useful for short-range structure refinement.

Atom-selective and use possible under various conditions (molecules, liquids, solids, interfaces, solutions...) also at low concentration

Advanced structural refinement is performed using multiple-scattering simulations (GNXAS)

Especially useful for disordered/ill-ordered matter (liquids, nanomaterials...) and dilute systems also under extreme conditions

Acknowledgements

Thanks for your attention!

Collaborators:

Camerino XAS group (recent): M. Minicucci, A. Trapananti, S. J. Rezvani, Y. Mijiti + students

National longstanding collaborations: A. Filipponi (L'Aquila), P. D'Angelo (Roma), S. Nannarone and G. Aquilanti (Trieste), C. R. Natoli (Frascati)

International collaborations: A. Polian (IMPMC Paris), F. Baudelet (Soleil Saclay), K. Hatada (Toyama Univ.), F. Iesari (Aichi Synchrotron), A. Witkowska (Gdansk)

Credits for several slides: A. Filipponi, P. Fornasini, B. Ravel, A. Witkowska, and more